

## 6. Material and Crystals from Mata Menge for Dating

### 6.1 Stratigraphy and sampling of material

The main scientific purpose of my trip to Mata Menge was to bring home material, which could allow me to determine the age of the archaeological artefacts collected over the last 50 years. This dating should take advantage of the argon mass spectrometer at Roskilde University. The  $^{40}\text{Ar}/^{39}\text{Ar}$  dating method had previously been a success for the excavation site at Wolo Sege. Mata Menge is the richest and most wellknown archaeological site in the Soa Basin and it is therefore important to know as accurate as possible, where it fits into the Palaeolithic period.

Three lots of material were brought home, each weighing 3 kg. The following measures give (compare figure 6.1) the precise position. Two lots were taken in the west baulk of trench no. 18. One of these lots, PL FLO11-01, was taken 7.2 m from the north end of the trench (14.27 m from the south end) at the height 80 cm from the bottom. The cross section of the digging was  $16 \times 20 \text{ cm}^2$  and the depth  $\sim 10 \text{ cm}$ . This lot is the one, which has now been dated and is described in the following. The second lot, PL FLO11-02, was also taken from the west baulk of the north-south going trench 1.8 m from the south end. The material is taken 139 cm from the bottom of the trench and the cross section was  $16 \times 20 \text{ cm}^2$  to a depth of  $\sim 10 \text{ cm}$ . The last lot of material, PL FLO11-03, was taken from trench 19, the east baulk, 1.8 m from the south end 38 cm from the bottom. The cross section was  $7 \times 31 \text{ cm}^2$  and the depth  $\sim 10 \text{ cm}$ . All these 3 lots of material were taken above the so-called sheet flow layer, where artefacts and most of the fossils were found. PL FLO11-02 was taken in a part of the trench, where the digging had not reached the sheet flow layer. PL FLO11-03 was taken above the sheet flow layer, which in this case was aligned with the bottom of the trench. The philosophy behind choosing these samples was to get a minimum age of the artefacts found. But so far only PL FLO11-01 has been studied.

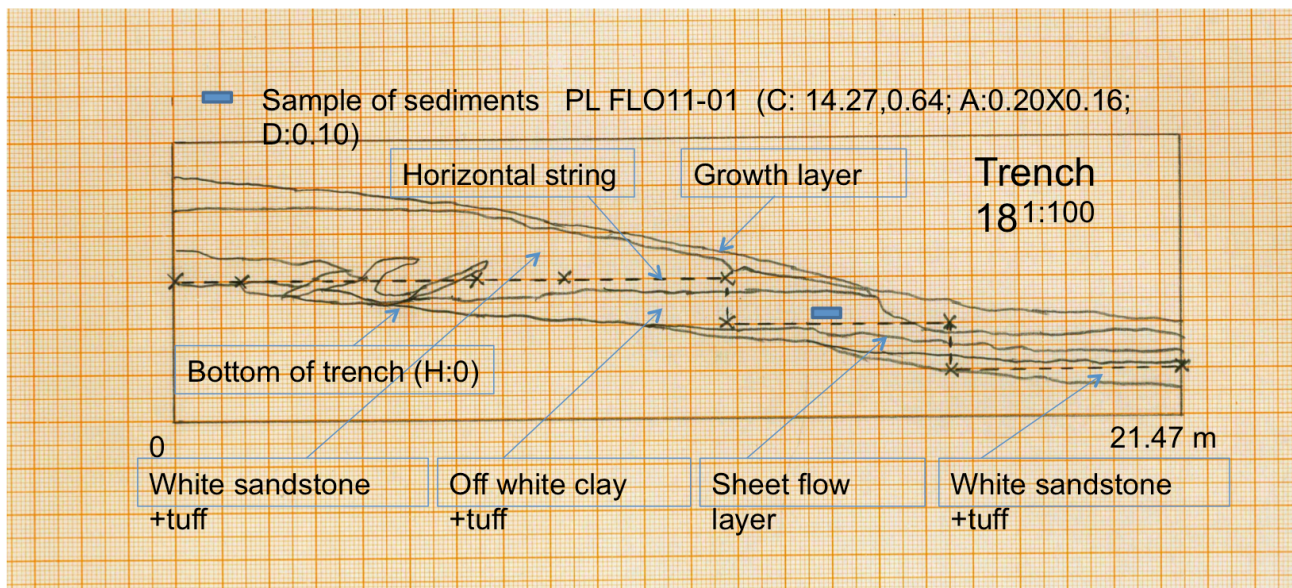


Figure 6.1. The stratigraphy of the west baulk of trench no. 18.

A complete set of photos of all the baulks of trench no. 18 and 19 was taken. Appendix A1 gives the 3x18 photos of the west baulk of trench 18. Figure 6.1 shows a drawing of the layers in the west baulk of trench no. 18. Figure 6.2 shows pictures of the section of trench no. 18, where the material for dating, PL FLO11-01, has been taken. One photo, Figure 6.2 (a), is before the material was dug out, but with marking of where the subsequent digging was made. Figure 6.2 (b) shows the

balk with the hole, where the material for dating has been taken. One clearly sees the sheet flow layer as the darker layer below the sandy ash layer, which has the rectangular hole. The few artefacts in trench 18 were according to the Indonesian archaeologists found with rather sharp positions in the sheet flow layer; this is opposite to for instance trench 27 and other trenches east of trench 19, where there is no sheet flow layer and both artefacts and fossils are found in a much wider depth regions as explained already in the last chapter.

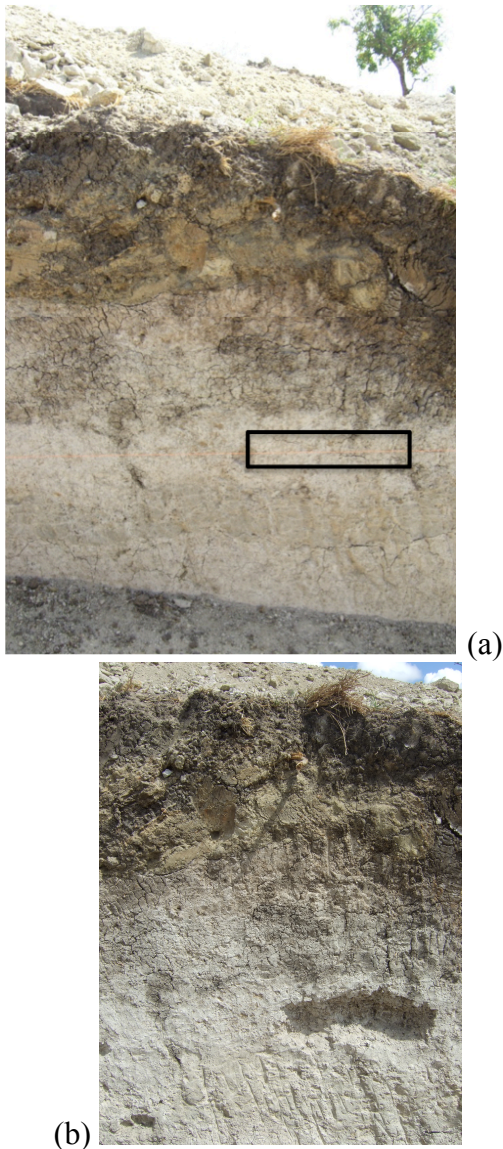


Figure 6.2. (a) West baulk of trench no. 18 before the material for  $^{40}\text{Ar}/^{39}\text{Ar}$  dating was taken. The four distinct layers are easily seen (for more description see figure caption to figure 6.3 and 6.4). (b) West baulk of trench no. 18 after the material has been dug out in a rectangle. (Photos: P.E. Lindelof).

4 layers were sampled from small holes close to the position where the material for dating was taken. Figure 6.3 (a) shows again the west baulk of trench 18, where the PL FLO11-01 material was removed. North of this rectangle 4 small holes were made in order to have material from each of the 4 layers that could be studied. The 4 layers are marked in figure 6.3 (b) with the numbers 1 to 4. The toplayer (1) is the topsoil and the upper tuffaceous sand layer with roots grown into it. The

layer (2) is tuffaceous sand layer with little structure, indicating that the ash has fallen on the water. The lack of turbulence structures indicates that the layer is not a deposit from streaming water but formed on the spot. The material for dating is taken from layer (2). Layer (3) is a deposit layer with various size stones formed by streaming water. It is in this layer that we find the stone artefacts and the fossil bones. In trench 18, however, very few fossils and artefacts are found. Layer (4) is another layer with ash and sand mixed into solid sandstone. The height position of the sheet flow layer is about 6 m above the corresponding layer at Wolo Sege.

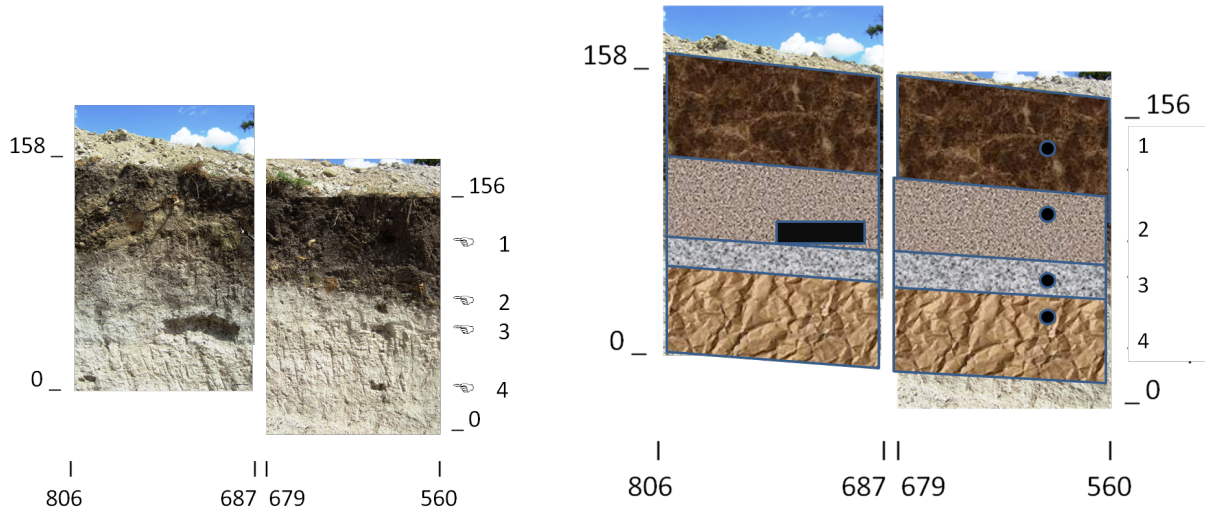


Figure 6.3 (a). Photo of the region of trench 18 baulk, where samples are taken for analyses.

(b). Illustration of the 4 different layers where Materials are taken.

The material taken from the 4 holes shown in figure 6.3 (b) were studied in a microscope after it was sieved with a grid with holes of size of 2.5 mm. This sieved material is microscopically displayed in figure 6.4 at different magnification. The particle size is not significant because it just reflect the mechanical work, which has been asserted to the brittle material. Layer (3) is much more finely divided, which is what one should expect of a sheet flow layer. It is layer (2), which is sieved and investigated in the following to take out individual crystals.

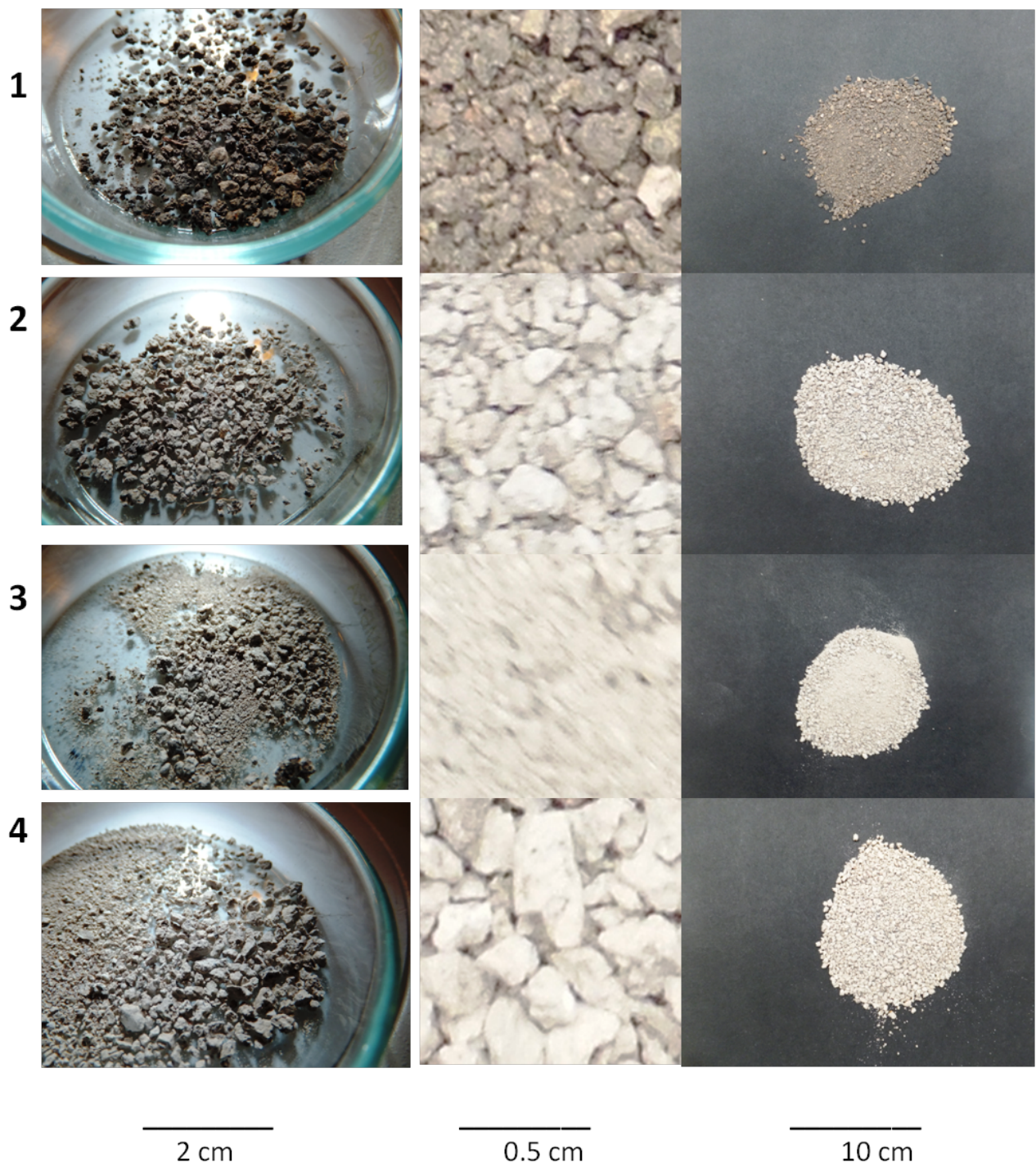


Figure 6.4. Material from the west baulk of trench no. 18 taken from the 4 different layers and close to the rectangular excavation used in the dating. Figure 6.3 (b) indicate the 4 small circular holes (1), (2), (3), and (4). 3 microscope pictures with different magnification are taken of each sample. Layer (2) is the tuffaceous sand layer from which the sanidine crystals used for the  $^{40}\text{Ar}/^{39}\text{Ar}$  dating are taken. Layer (3) is the sheet flow layer where artefacts and fossil bones are found.

## 6.2 Two important potassium-rich volcanic crystals

The  $^{40}\text{Ar}/^{39}\text{Ar}$  dating method [McDougall 1999] requires crystals, which at the time of archaeological interest has lost all argon accumulated by the decay of potassium, the radiogenic argon. The dating of the human activity is based on crystals created by a volcanic eruption. Volcanic eruption yields a large number of crystals, which are spread with the volcanic ash or lava [Philpotts et al. 2009]. Only dense crystals containing potassium in the pct range are suitable. The crystals containing potassium as part of the chemical structure are not uncommon, but the crystal structure must also be compact in order to avoid the argon diffusing away. The measurement method requires crystals weighing tens of mg, preferably more than around 100 mg to get the best accuracy. Single crystals are the best because argon may diffuse along grain boundaries. But polycrystalline materials are often the only materials available and can easily be used, in particular if some precautions are taken during the mass spectrometer measurements (see chapter 8 p. 46).

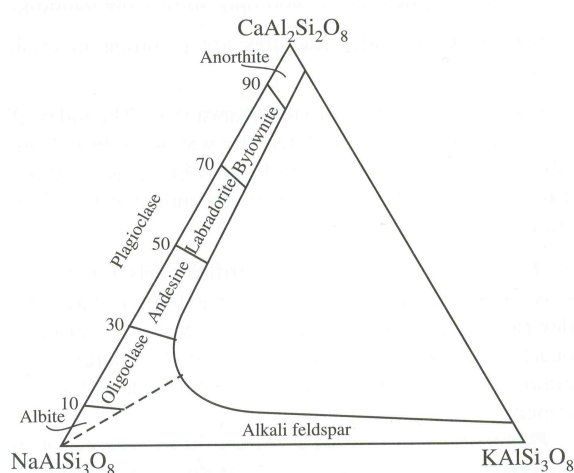
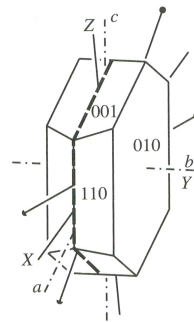


Figure 6.5 Composition triangle for feldspars [Nesse 2004 p. 134]

The most suitable type of crystals for  $^{40}\text{Ar}/^{39}\text{Ar}$  dating is sanidine [Nesse 2004 p. 148]. Fortunately this type of crystal exists in the volcanic ash layers in Mata Menge, which we want to date. Sanidine belongs to the Aluminiumsilicate crystals, which appears in chemical combination with calcium, sodium and potassium. They are called the plagioclase and the alkali feldspar and are often plotted in a triangular diagram, as shown in figure 6.5. They all look similar and have the triclinic crystal structure. They are often transparent, but can have many colours. They are difficult to separate, because they have almost the same density and they are non-magnetic. Only the potassium rich crystals ( $\text{KAlSi}_3\text{O}_8$ ) in the lower right corner of the triangle in figure 6.5 are useful for the  $^{40}\text{Ar}/^{39}\text{Ar}$  dating. They are called sanidine crystals and shown in figure 6.6 (a). Modern X-ray luminescence spectroscopy (XRF) has offered a method to separate sanidine crystals from the other silicates and from quartz. Quartz crystals are common in the ash layers at Mata Menge, but are recognizable because they have a simple tetragonal crystal structure and never contain potassium.



(a)



(b)

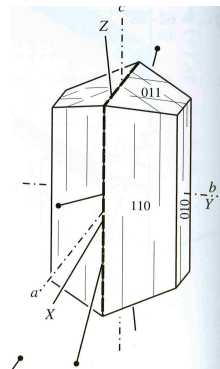
Figure 6.6 (a) sanidine single crystals (picture is 5 mm high). [web address WWW1]

(b) Sanidine Wigner Seitz cell (triclinic). [Nesse 2004, p.144]

Another type of crystal suitable for  $^{40}\text{Ar}/^{39}\text{Ar}$  dating is the so-called hornblende crystal. It has the chemical composition  $(\text{NaK})_{0-1}\text{Ca}_2(\text{MgFeAl})_5(\text{SiAl})_8\text{O}_{22}(\text{OH})_2$  and has monoclinic crystal structure (the unit cell is shown in figure 6.7 (b)). Hornblende crystals are found in the ash at Mata Menge and with their black appearance as seen in figure 6.7 (a), they are easy to find under a microscope in the ash. It may only contain small amount of potassium. Because in 2008 the Quadlab did not have a XRF equipment, the studies of material from Wolo Sege by Gitte M. Jensen for the  $^{40}\text{Ar}/^{39}\text{Ar}$  dating was based on hornblende crystals, which is relatively easy to pick out by hand [Brumm et al. 2010a].



Figure 6.7(a) Hornblende single crystals. [web address WWW2]. Longest crystal is ~5 mm.



(b) Hornblende Wigner-Seitz cell (monoclinic) [Nesse 2004, p. 208]

### 6.3 Sieving and sorting of the PL FLO11-01

On the basis of the 3 kg of material, PL FLO11-01, from trench 18 crystals suitable for  $^{40}\text{Ar}/^{39}\text{Ar}$  analysis were extracted. This was done in 3 separate processes: 1) sieving, 2) magnetic separation, and 3) XRF analysis. First we made a sieve into several lots by 6 different sieves leaving size lots as given in table 6.1. The 5 sieves were inserted in a shivering machine for 15 minutes. The stack of stainless steel sieves are seen in figure 6.8, where also plastic bags with the grains and cleaning brushes for the sieves are seen.



Figure 6.8. Sieving equipment in the processing laboratory. The column with 5 stainless steel sieves are seen on the table together with the important cleaning brushes and a tweezer, which are subsequently used in the cleaning process. (Photo: P.E. Lindelof)

Only the size ranges 0.315-0.5 mm and 0.5-1 mm in the sieving process were useful, because we subsequently made a magnetic separation, in a so-called Frantz Magnetic Separator seen in figure 6.9, which could only take these sizes of crystals.

PL-FLO11-01,		1.5 kg (out of totally 3 kg)			
>4.0 mm	700 g	mechanical			
2.0-4.0 mm	400 g	mechanical			
1.0-2.0 mm	~200 g	mechanical	1.0-2.0 mm	Ultra, wetsieved	30 g
combined			0.5-1.0 mm	Ultra, wetsieved	
			0.315-0.5 mm	Ultra, wetsieved	
			0.150-0.315 mm	Ultra, wetsieved	
			0-150 mm	Ultra, wetsieved	30 g
0.5-1.0 mm	120 g	mechanical	<80 mA, 10°	magnetic	8g (incl.strong magnetic)
combined combined			80 mA-0.2 A, 10°	magnetic	6 g
			0.2 A-0.5 A, 10°	magnetic	60 g
			0.5A-1.0A, 10°	magnetic	30 g
			1.0A-1.8A, 10°	magnetic	4 g
			>1.8A, 10° & 5°	magnetic	1 g
			>1.8A, 10° & 5°	Non-magnetic	0.5 g
0.315-0.5 mm	90 g	mechanical			
0-0.315 mm	160 g	mechanical			

Table 6.1. The amount of different size lumps of material after sieving and the result of magnetic sorting of the ash lumps and crystals. Only 0.5 g out of 1500 g starting material was non-magnetic.

The sand/ash material was lumpy, and to obtain as many crystals from the ash as possible, the material was not only dry-sieved, but also wet-sieved to take the lumps to pieces. The result of this was 120 g out of the 1500 g became crystals and ash lumps in the 0.5-1 mm size range. It was treated in an ultrasound bath and the fine powder was poured out and the crystals were dried to get ready for the magnetic separator.

The principle of the magnetic separator, figure 6.9, is to let the particles smaller than 1 mm slide down a plastic rail with a generated sound wave that helps moved them along. While they slide down the rail the particles are forced perpendicular to their sliding direction by a perpendicular slope. However an electromagnet assures no perpendicular move of the strongest magnetic particles and the flow of particles are therefore divided into two streams of particles. The magnetic field is changed in steps and the least magnetic particles are sliding down the rail again in a higher magnetic field. Gradual sorting of particles depending on their magnetic dipole strength avoids a lumping of magnetic particles and assures a true individual sorting according to their magnetic dipole strength. Table 6.1 gives the weight of each class of sizes of magnetic particles. In the end the perpendicular slop is decreased to 5°, as indicated on the table, and those which are unaffected by the strongest magnetic field (corresponding to 1.8 A through the electromagnet) is characterized as non-magnetic. Out of the 1500 g of material only 0.5 g is collected as non-magnetic crystals. It is this 0.5 g of non-magnetic crystals, which contains the sanidine crystals.



*Figure 6.9. The Frantz magnetic separator. A sound wave activates the crystals in the small funnel at the upper right down along a plastic rail to the two containers seen to the left. The electromagnet creates a field gradient, which separate the flow of crystals into the two containers according to their magnetic properties. (Photo: P.E. Lindelof)*

#### **6.4 Choosing sanidine feldspar crystals by XRF**

The approximately 1 g (out of totally 3000g PL FLO1101 material) of non-magnetic crystals contains lumps of ash, crystals and crystals combined with solid ash lumps. To further isolate the crystals this material was cleaned again with ultrasound in deionized water and then crystals were

picked with a tweezer under a microscope and placed on a sample holders with a 5x12=60 squares of 3.5x3.5 mm. The sample holder with the crystals in position was sprayed with acetone glue in order for the crystals not to move around. Figure 6.10 shows a little part of such a sample holder with crystals in position.

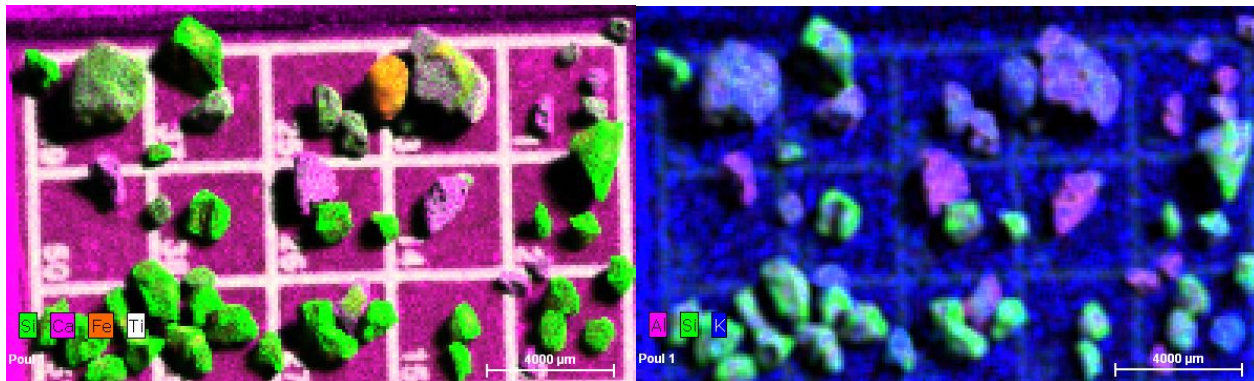


Figure 6.10. An XRF measurement on non-magnetic crystals. The atomic spectral analysis highlights Si, Ca, Fe, and Ti to the left and Al, Si, and K to the right.

These frames with crystals were placed in a M4 Tornado  $\mu$ -XRF instrument [M4 Tornado Manual 2009] shown in figure 6.11 and the X-ray fluorescence of the frame allowed to display the element composition of each crystal. The frame with the crystals can be shown in colours in the computer screen coded to particular elements. Figure 6.10 shows a particular set of crystals with two different colour settings on the XRF. Each XRF measurement shows the colour of the crystals corresponding to an average colour of the crystals. Displaying two computer representations of the atomic composition makes it possible to determine the elements in the crystal basis. When this XRF measurement has been taken the frame with the crystals are again taken out of the sample chamber and the crystals which contain considerable amount of K is removed from the frame and placed in a small aluminium sample holder (figure 7.1) made for neutron irradiation procedure. Out of the 3 kg of PL FLO11-01 material 24 sanidine crystals were found, - a fair number for a  $^{40}\text{Ar}/^{39}\text{Ar}$  dating.



Figure 6.11. The M4 Tornado  $\mu$ -XRF instrument from Bruker Co. (Photo: P.E. Lindelof).

## 7. Neutron Irradiation-Induced Decay of Potassium Isotopes.

### 7.1 Decay of radioactive elements

Radioactive decay of atomic nuclei today forms the basis of prehistoric dating.  $^{14}\text{C}$  dating was discovered by Lippy [Andersen et al. 1947] immediately after Second World War II and has since dominated the chronology of the evolution since the start of the Upper Palaeolithic Stone Age from  $\sim 40$  ka before present (BP).  $^{14}\text{C}$  is formed by cosmic radiation from the stable and most abundant carbon isotope,  $^{12}\text{C}$ , of the  $\text{CO}_2$  in the atmosphere and incorporated in all organic material. When first incorporated in the biological materials the  $^{14}\text{C}$  decays with a half life of 5730 years. Consequently there is a limit to how long back in prehistoric time we can use this method ( $\sim 40,000$  years). The concentration of  $^{14}\text{C}$  in the atmosphere is kept roughly constant by the intensity of the cosmic radiation. However the cosmic radiation is determined by events in the solar system, in particular the sunspots, and the generations of  $^{14}\text{C}$  are therefore fluctuating, leading to sometimes fairly uncertain age determination, which rely then on tree ring calibrations, which is only reliable 10,000 years back.

The most reliable radioactive dating methods are based on the natural concentration of radioactive isotopes incorporated in the earth mantle at the creation of the earth 4.6 billion years ago. Obviously only radioactive isotopes with a lifetime comparable to this value are still in existence and thus useful. Decay times of radioactive isotopes with an age comparable to that of the earth, can, thanks to today's high accuracy of element concentration measurements, be used in the full prehistoric period (2.5 million to 2000 years BP), though with decreasing accuracy.

2000 years of decay of  $^{40}\text{K}$  give 0.12 ppm.  $^{40}\text{K}$  has a concentration of 0.0117% of the total K-atoms and the relative concentration of potassium in sanidine is typical 1%. Thus only  $1.2 \cdot 10^{-10}$  % of the sanidine weight will show up as  $^{40}\text{Ar}$ . The crystals we are investigating weigh typically 1 mg and the total mass we must detect is therefore  $1.2 \cdot 10^{-15}$  g or  $3 \cdot 10^{10}$  atoms. A challenging but not impossible number.

An age determination requires a starting point at the archaeological event of interest from where to count the number of decays. This can be a simultaneous volcanic event or a heating of some material in the fire by a Stone Age human. Suited materials are only  $^{40}\text{K}$  (1250 Ma) and  $^{238}\text{U}/^{235}\text{U}$  (4470 Ma/704 Ma). Another method beside the argon-argon method is to measure tracks of high-speed nuclei emanating in a fission event of  $^{238}\text{U}$  (8200000 Ma). These tracks will be erased by heating, but otherwise measurable as tracks in the surface of a crystal with incorporated constant concentration of fission elements. This dating method requires only simple polishing methods and a standard optical microscope and is therefore quite commonly used, also at the sites of the Soa Basin. The fission track dating method is however not very reliable, since fission tracks in all directions measured at a surface of a crystal is difficult to count.

To determine the age on the basis of the measured  $^{40}\text{Ar}$  requires basically 2 things: 1) that we know the original number of  $^{40}\text{K}$  atoms and 2) that we know how much  $^{40}\text{Ar}$  there was a priori in the sample (indiffused from the atmosphere, while the sanidine crystal was hot). The last number is extrapolated from the amount of  $^{36}\text{Ar}$ , which comes only from the atmosphere. The first number is difficult to measure accurately, since the  $^{40}\text{K}$  is strongly bound; it is therefore convenient that we can determine the number of  $^{36}\text{Ar}$  atoms by an irradiation in a nuclear reactor [Dalrymple 1981] as we shall discuss in section 7.3.

## 7.2 Radioactive decay of <sup>40</sup>K

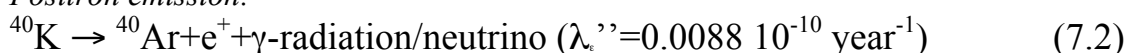
Potassium (K) has two stable isotopes, <sup>39</sup>K and <sup>41</sup>K, and only one radioactive isotope, <sup>40</sup>K, with a geological half time of 1250 million years. The abundances of <sup>39</sup>K and <sup>41</sup>K are 93.2581% and 6.7302%. The abundance of <sup>40</sup>K decrease over the timescale of the earth and it is today ¼ of the value it had at the creation of the earth. On an archaeological timescale the abundance is however for all practical circumstances constant with a value of 0.01167%. All the abundances of the potassium isotopes are each known with relative accuracies of 0.03-0.3% [Garner et al. 1975] which are adequate for our subsequent analyses.

<sup>40</sup>K decays by 3 different nuclear processes:

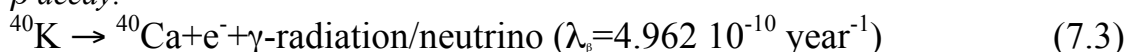
*Electron capture:*



*Positron emission:*



*β-decay:*



$\lambda_e = (\lambda_e' + \lambda_e'')$  and  $\lambda_\beta$  are the decay constants for the decay to <sup>40</sup>Ar and <sup>40</sup>Ca respectively and are proportional to the decay probabilities. As seen the most common decay of <sup>40</sup>K is to <sup>40</sup>Ca. The total energy of the electron and the γ-radiation/neutrino is 1.46 MeV. The decay to <sup>40</sup>Ar is 9.54 times less frequent than to <sup>40</sup>Ca and the energy of the γ-radiation/neutrino is in this case 1.26 MeV. In the case of the two decay routes to <sup>40</sup>Ar the decay constant is the sum of two individual decay constants,  $\lambda_e' + \lambda_e'' = 0.581 \cdot 10^{-10} \text{ year}^{-1}$ . The time it takes to half the number of <sup>40</sup>K atoms is given by the expression

$$t_{1/2} = \ln 2 / \lambda = 1.25 \cdot 10^9 \text{ years} \quad (7.4)$$

$$\text{where } \lambda = \lambda_\beta + \lambda_e' + \lambda_e'' = 5.543 \cdot 10^{-10} \text{ year}^{-1}. \quad (7.5)$$

## 7.3 Accumulation of the decay products in solid materials

After the decay of <sup>40</sup>K the decay products, <sup>40</sup>Ar and <sup>40</sup>Ca, become incorporated in the material, which contained the potassium in the first place. Whereas the calcium atoms become strongly bound to the material, either as covalently or interstitially, the argon atoms will be much more loosely bound interstitially, because argon is an inert gas and furthermore because the <sup>40</sup>Ar atoms are relatively large compared to the lattice constant of most crystals. In some very weak-binding crystals the argon atoms may actually diffuse out of the material at room temperature. However in more dense materials the argon atoms cannot be moved around by the thermal agitation at room temperature and in crystal structures like Hornblende and feldspar, which is important in dating investigations at Soa Basin, temperatures of 400 °C is needed to get the argon diffusing, and a complete melting of the materials (800°C) is necessary to drive all the argon out of the crystal. Such high temperatures are naturally only occurring at the surface of the earth at volcanic eruptions. The <sup>40</sup>Ar/<sup>39</sup>Ar dating method is therefore performed on crystals in volcanic ash material layered relative to archaeological artifacts or human and animal fossils. Fortunately several volcanic crystals contain sufficient amount of potassium and are sufficiently dense and hard, so that argon from the decay is trapped inside the crystal. Hornblende and sanidine (feldspar) crystals are among the most

suitable. Hornblende crystals were used [Brumm et al. 2010a] for the dating of the Wolo Sege artifacts. Sanidine crystals were used in the present study.

As we shall see in the following not all dating data is to be understood in a straightforward way. The fundamental way of understanding such deviation is based on diffusion theory. The argon atoms are moving around in the crystal as a high velocity ball in a hilly landscape. The temperature gives the distribution of the velocity of the argon atoms. The higher the velocity the easier it is for the argon atoms to overcome the (potential) hills. The perfect crystal's built-in crystal field gives the basic potential landscape, but there are also important contribution from faults and impurities. The potential hills may vary considerably between different parts of the crystal, and the movement (diffusion) of the argon atoms in some part of the crystal may significantly vary from another part of the crystal. This is amplified by the fact that the diffusion is exponentially dependent on the potential landscape and the temperature.

When the volcanic crystal (e.g. sanidine) is formed during a cooling process, atmospheric argon diffuses into the crystal in ways, which depend on the speed of cooling and the inhomogeneity of the crystal forming. The distribution of atmospheric argon in the crystal can for this reason be quite complicated. After a long time, when a significant part of the  $^{40}\text{K}$  has decayed, a heating of the crystal may change the distribution of argon in the crystal in a quite complicated way. For instance a complicated situation may occur, if the crystal is formed in one volcanic eruption and then again heated partially in a subsequent eruption (this is called a xenon crystal). All these complicated distributions of argon in the excavated crystals must be understood in principle, but does not preclude using the crystals for dating.

#### 7.4 Neutron irradiation-induced decay of $^{39}\text{K}$ in a nuclear reactor

The first usage of volcanic crystals containing potassium for age determination only involved knowledge of the concentration,  $N$ , of the parent isotopes ( $^{40}\text{K}$ ) and the concentration,  $D$ , of the argon daughter isotopes ( $^{40}\text{Ar}$ ), where the original concentration of parent isotopes then are  $N_0 = N + (\lambda / (\lambda_e + \lambda_c))D$ , with the known total decay constant  $\lambda = \lambda_e + \lambda_c + \lambda_\beta$ . The following simple expression for the age,  $t$ , of the crystal emerges:

$$t = \lambda^{-1} \ln(1 + (\lambda / (\lambda_e + \lambda_c))D / N) \quad (7.6)$$

It was soon realized, however, that this was much too simple in the case of  $D/N = ^{40}\text{Ar}/^{40}\text{K}$  to give an accurate age. The most important correction comes from the presence of  $^{40}\text{Ar}$  from indiffused air into the sample, which must be subtracted to get the concentration of the radiogenic argon,  $^{40}\text{Ar}^*$ , to be substituted for  $D$  in eq. (7.6).

Another difficulty was to determine the absolute concentration of  $^{40}\text{K}$  in the samples, since potassium is strongly bound and must be determined in a completely different process than the argon isotopes. This was solved by converting  $^{40}\text{K}$  into  $^{39}\text{Ar}$  by neutron activation in a nuclear reactor according to the nuclear reaction



where  ${}^1_0\text{n}$  is a neutron, and  ${}^1_1\text{p}$  is a proton. The product,  $^{39}\text{Ar}$ , has a half lifetime of 269 years, which is sufficiently long to make subsequent mass spectrometric measurements. By measuring  $^{39}\text{Ar}$  we get a proportional amount of  $^{39}\text{K}$ , and due to the universal ratios of the three potassium isotopes  $^{39}\text{K}$  (93.26%),  $^{40}\text{K}$  (0.0117% (today)) and  $^{41}\text{K}$  (6.73%), we may determine  $^{40}\text{K}$ . The concentration of  $^{40}\text{K}$

can then be determined absolutely by measuring the neutron flux or by comparing with a known reference (as we do in the following).

Our samples and references were mounted in an 18 mm diameter sample holder, figure 7.1, made of aluminium and placed in the center of a Nuclear reactor of the type TRIGA at the Oregon State University, USA, with a maximum power of 8 MW. It is a heavy water moderated enriched  $^{235}\text{U}/^{238}\text{U}$  reactor with high-energy neutron flux in the center of the reactor [Dalrymple 1981]. The neutrons do not generate high radioactivity in aluminium. Cadmium tubes (the so-called CLICIT facility) guide our aluminium sample holder into the center of the reactor core. The cadmium acted to absorb the thermal neutron flux and leave mostly the high-energy neutron for the irradiation of our samples from Mata Menge. This is practical, since it is the high-energy neutrons, which most effectively generate the process eq. 7.6.

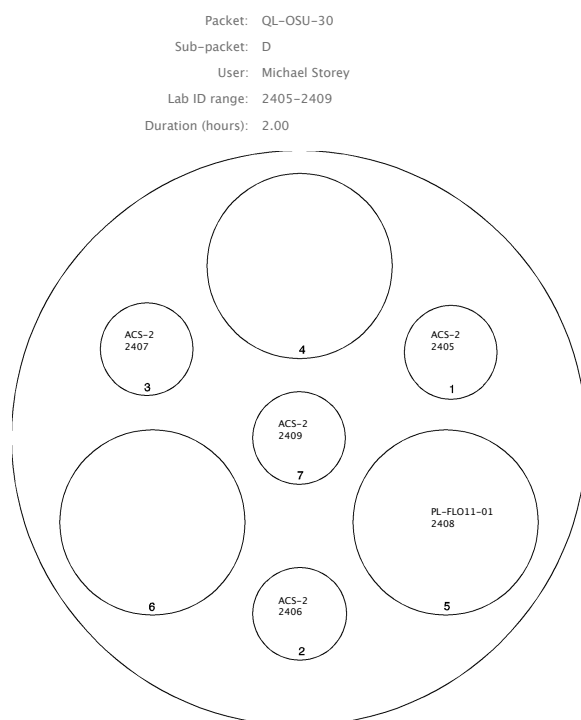


Figure 7.1. Aluminium sample holder for neutron irradiation in the nuclear reactor at Oregon, USA. The diameter is 18 mm. The 4 small 10 mm deep drilled holes (2405, 2406, 2407, 2409) contain each 8 reference samples (ACS 1-4, 1.194 Ma) from Alder Creek for calibration of the 24 sanidine crystal samples from Mata Menge (PL-FLO11-01) placed in hole number 2408. The neutron fluence at 2408 was extrapolated from the 4 reference positions.

The high fluence of neutrons generates a large number of different processes in the samples, many leading to argon isotopes. Fortunately most of these interferences are insignificant. The only important process is the generation of  $^{36}\text{Ar}$  from  $^{40}\text{Ca}$  because precisely  $^{36}\text{Ar}$  is used for compensating for atmospheric argon in the sample. The neutron induced  $^{36}\text{Ar}$  can however in turn be found from measuring the  $^{37}\text{Ar}$ , which is predominantly created from  $^{40}\text{Ca}$  and allows to determine the  $^{36}\text{Ar}$  generated by the neutrons. Thus a simple process of finding the original  $^{40}\text{K}$  and

the radiogenic  $^{40}\text{Ar}^*$  can be fully implemented from measurements of  $^{39}\text{Ar}$ ,  $^{37}\text{Ar}$  and  $^{36}\text{Ar}$ . Of course also the so-called blank measurement must be performed in order to check any erroneous background in the mass spectrometer. I will describe this later.

## 8. The Physical Principles of Argon Age Determination

### 8.1 $^{40}\text{Ar} / ^{39}\text{Ar}$ dating method

Measuring a sanidine sample from Alder Creek (ACS) in the USA for which we have already the age and other information and which we include in the neutron activation together with the unknown samples greatly facilitate the data analysis and improve our accuracy. By suitable manipulation we determine  $^{40}\text{Ar}^*$ , the natural radiogenic isotope, and the mother isotope,  $^{40}\text{K}$ , represented by the  $^{39}\text{Ar}_K$  isotope formed by the neutron irradiation from  $^{40}\text{K}$ .  $^{39}\text{Ar}_K$  has a decay time of 269 days. This allows us to write the age of a sanidine (or any other crystal as for instance hornblende) in the following form [McDougall 1999]:

$$t = \lambda^{-1} [1 + J(^{40}\text{Ar}^*/^{39}\text{Ar})] \quad (8.1)$$

Where  $\lambda^{-1} = 1250$  million years and

$$J = [e^{\lambda t_0} - 1] / (^{40}\text{Ar}^*/^{39}\text{Ar}_K) \quad (8.2)$$

Where  $t_0 = 1.194$  Ma is the age of the predetermined sanidine reference ACS sample.

### 8.2 The step-heating method

One of the advantages of transforming the concentration of potassium isotopes into a measurement of argon isotopes is that measurements of the 4 argon isotopes,  $^{36}\text{Ar}$ ,  $^{37}\text{Ar}$ ,  $^{39}\text{Ar}$  and  $^{40}\text{Ar}$ , for any part of a sanidine crystal or any partial heat release of argon give the age of the sample. The sample is therefore heated in smaller steps and the age determined in each case. Figure 8.1 shows an example of such a stepwise heating and release of argon isotopes yielding the apparent age of the sample from each set of argon measurements. The results in figure 8.1 are from one of the most accurate and consistent measurements (sample 2408-02). In the next chapters the experimental details and a full account of my measurements and age determination will be given.

For each of the 5 heatings the age has been determined from eq. (8.1) and plotted as a function of the cumulative  $^{39}\text{Ar}$  released, given in percent of the total release. The accuracy is given by the width of the line around the mean value of the age. The mean square accuracy is determined from the accuracy of all the measurements used in the age determination by a least square method. An age determination based on a smaller release of  $^{39}\text{Ar}$  gives a larger least square standard deviation. Important in figure 8.1 is the fact that all partially determined ages are within each other's standard deviations. This is the case in figure 8.1, but may not always be the case. Several reasons for such failures can be given and arguments given for which of these numbers are most trustable. In figure 7.1 we have indicated the totally integrated age value by adding all argon release and an average given by a least square sum of the 5 weighted individual step heating measurements. It is difficult to argue which of these numbers are most relevant and they are often as here within each other's standard deviation.

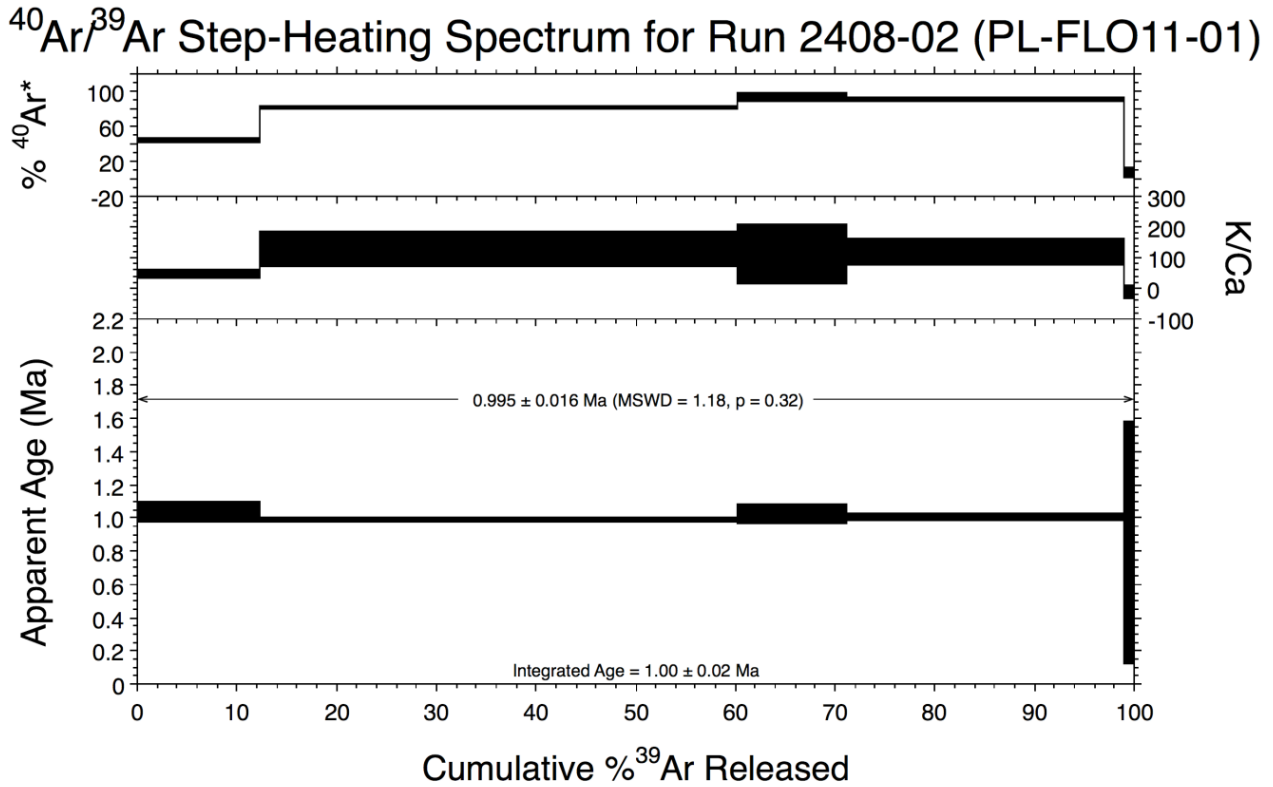


Figure 8.1. Step heating result for crystal no. 2408-02 from the PL FLO11-01 excavation.

In figure 8.1 I also give values of the ratio of potassium to calcium concentration in the sample. A high number means that the correction to the  $^{36}\text{Ar}$  amount from the neutron activated decay of Ca is small and the determination of the radiogenic argon,  $^{40}\text{Ar}^*$ , more accurate. The ratio for sanidine is high relative to many other crystals, such as hornblende. The percentage of the totally released radiogenic argon in the subsequent 5 heatings is given in the plot in the top of the figure and shows for instance why the inaccuracy of the last heating is large, because the amount of  $^{40}\text{Ar}^*$  is small (as is  $^{39}\text{Ar}$ ).

### 8.3 The isochron consistency

A very useful consistency plot is the so-called isochron, meaning a plot, which for one age value should give a characteristic straight line [McDougall 199 p. 112]. It is a plot where each heating step gives a data point with the coordinates  $(^{39}\text{Ar}/^{40}\text{Ar}, ^{36}\text{Ar}/^{40}\text{Ar})$ . It is seen in figure 8.2 that the deviation of the points is given mostly by the uncertainty of the  $^{36}\text{Ar}$  concentration. The 5 heating steps of sample 2408-02 fall on a straight line, where the slope and the point where the line crosses the abscissa axis both gives the accumulated age value for the sample. The crossing of the line with the ordinate axis gives a consistency check on the ratio of the atmospheric values of  $^{36}\text{Ar}$  and  $^{40}\text{Ar}$ . How to understand the importance of this isochron plot will be outlined now.

To understand the significance of the coordinates in figure 8.2, I write them in the following way:

$$X = \frac{^{39}\text{Ar}}{^{40}\text{Ar}} = \alpha(t) \frac{^{40}\text{Ar}^*}{(^{40}\text{Ar}^* + ^{40}\text{Ar}_{\text{air}})} = \alpha(t) \frac{^{40}\text{Ar}^*}{(^{40}\text{Ar}^* + 395 \text{ } ^{36}\text{Ar})} \quad (7.3)$$

Where  $^{40}\text{Ar}_{\text{air}}$  is the indiffused argon from the atmosphere.

$$Y = {}^{36}\text{Ar}/{}^{40}\text{Ar} = {}^{40}\text{Ar}_n/395({}^{40}\text{Ar}^* + {}^{40}\text{Ar}_n) = {}^{40}\text{Ar}_n/395({}^{40}\text{Ar}^* + 395 {}^{36}\text{Ar}) \quad (7.4)$$

Or

$$Y = -\alpha(t) X \quad (7.5)$$

where

$$\alpha(t) = {}^{39}\text{Ar}/{}^{40}\text{Ar}^* = J/(e^{\lambda t} - 1) \quad (7.6).$$

$\alpha(t)$  is a constant for a given crystal. For  $X=0$ ,  ${}^{40}\text{Ar}^*$  must be 0 and  $Y=1/395$ .

For  $Y=0$ ,  ${}^{36}\text{Ar}$  must be 0 (no air) and  $X=\alpha(t)$ , which represents the age (like the slope).

All points on the sloping line eq. (7.5), represent the same age (isochron), and the fact that all point within the uncertainty is on the line gives confidence to the crystal and the consistency of the data.

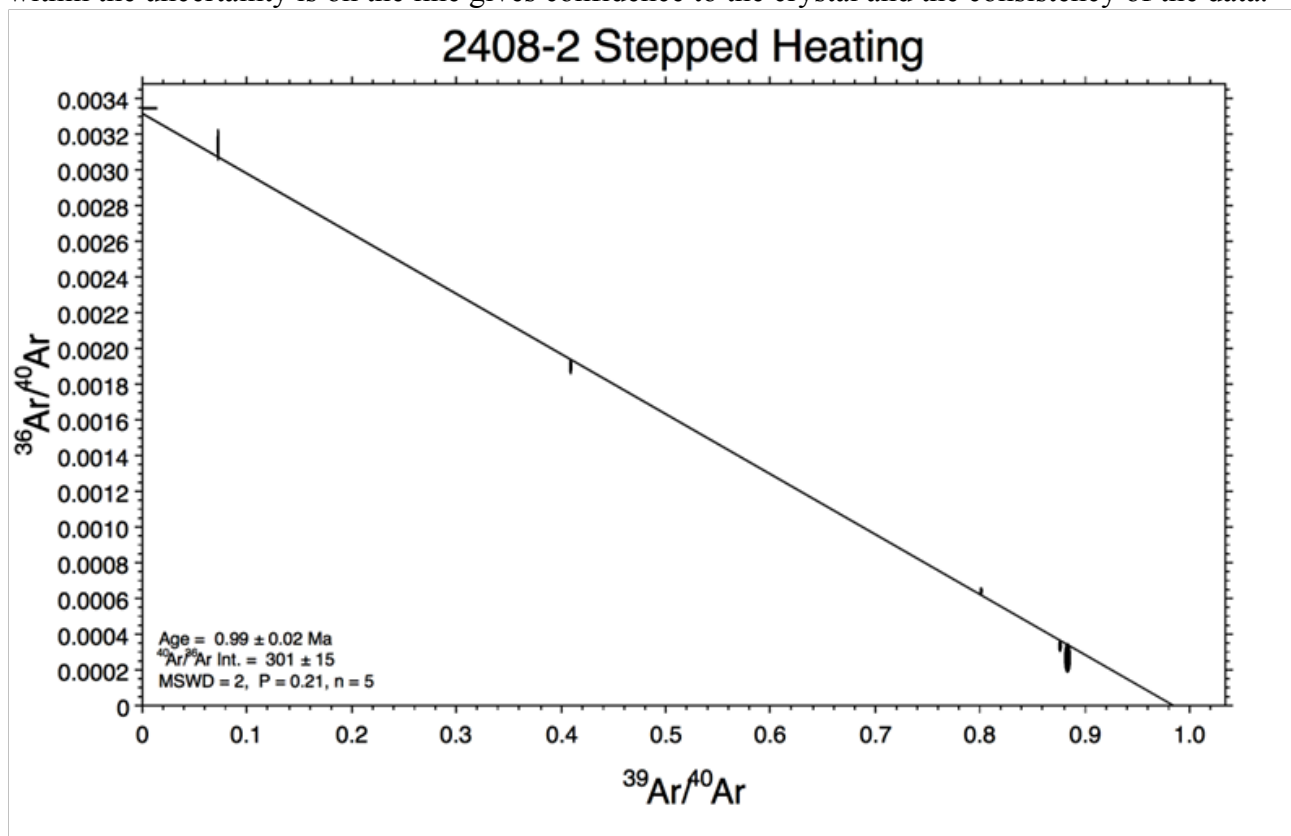


Figure 8.2. The isochron for crystal 2408-02. All 5 step-heating points lie on the straight line representing the age of the sample. The crossing of the line with the y-axis gives the value 301 and this is consistent with the value 295 within uncertainties. The age is given by the slope of the line and has an uncertainty of 2%, as well as given by the crossing of the line with the x-axis.

## 9. The Argon Mass Spectrometer

### 9.1 Crystal mounting

After the samples and references have been irradiated with high energy neutrons for 2 hours in Oregon they are stored for a couple of months for the minor induced radioactivity to become insignificant. The decay time of  $^{39}\text{Ar}$  is 269 days, so most of this isotope is kept and we can extrapolate back to the concentration of  $^{39}\text{Ar}$  at the time of the neutron irradiation. The samples are then moved to a new aluminium sample holder shown in figure 9.1 from the sample holder for the neutron irradiation, figure 7.1.

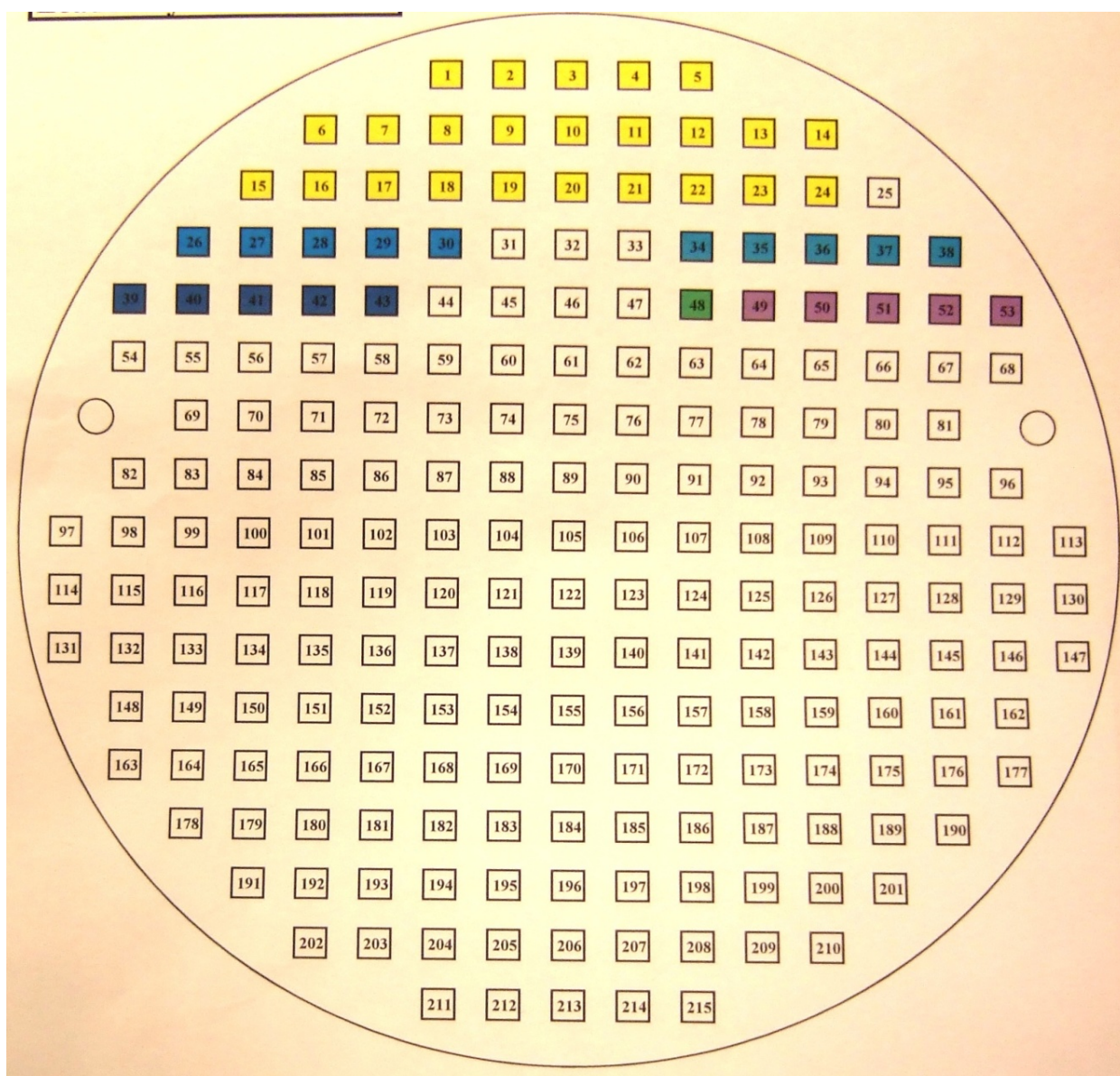
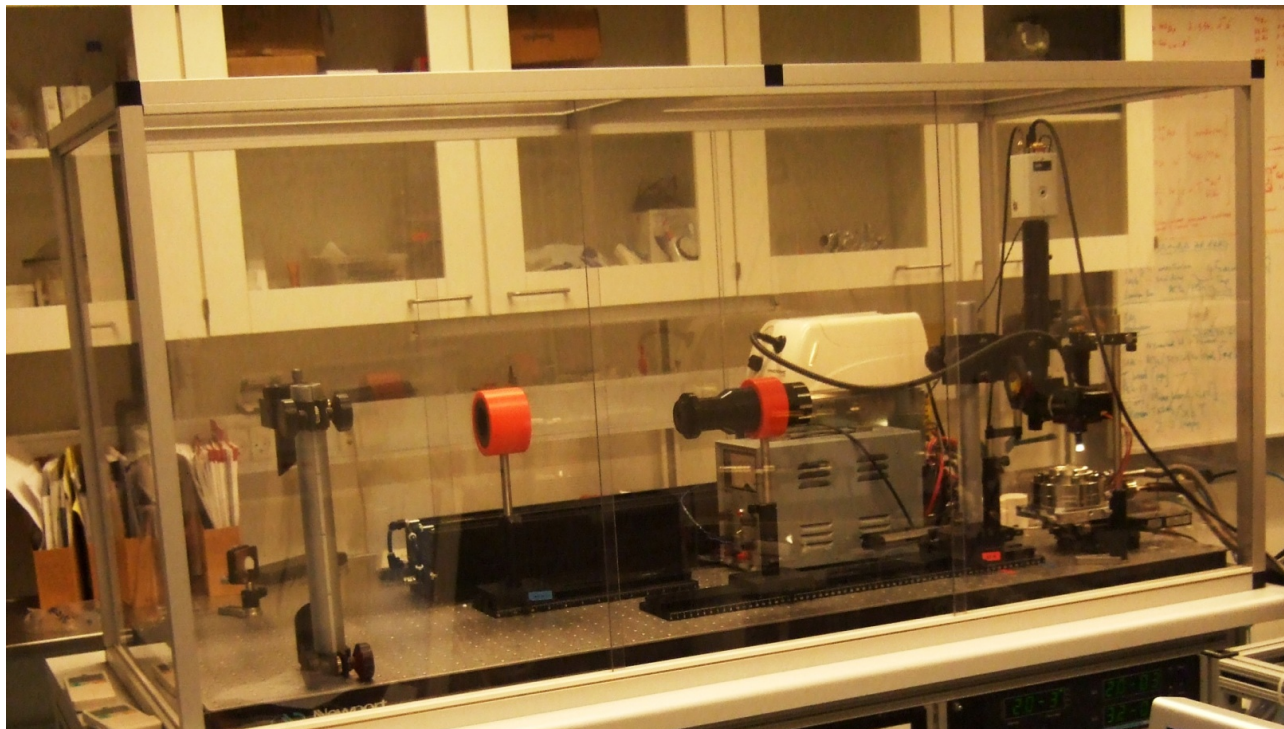


Figure 9.1. Sample holder for the argon mass spectrometer. Each of the square holes can be reached by the focused  $\text{CO}_2$  laser radiation by a servomotor in the  $x$  and  $y$  direction.

The 24 samples or crystals are mounted in hole 1 to 24 and are named with the crystal numbers 2408-01 to 2408-24. The 20 reference (Alder Creek) crystals are mounted in hole 26-30, 34-38, 39-43 and 49-53 and are divided according to where they have been situated (2405, 2406, 2407, 2409) during the neutron irradiation as shown in figure 7.1.



*Figure 9.2. CO<sub>2</sub> laser with mirrors and the argon spectrometer crystal mount (to the right), with vertical video camera (monitor is seen in figure 9.7). The CO<sub>2</sub> laser beam can be focused to 10  $\mu\text{m}$  diameter. A programmed step motor addresses each of the crystals. (photo: P.E. Lindelof).*

## 9.2 CO<sub>2</sub> laser set-up and heating

The sampleholder for the spectrometer is mounted in a special holder seen in the lower right part of the laser plexoglass box figure 9.2. It is part of the ultra-high vacuum of the spectrometer. A ZnSe single crystal plate is transparent for 10  $\mu\text{m}$  radiation from a CO<sub>2</sub> laser. During the later heating of the samples small amount of material evaporates from the sanidine crystals and to avoid contaminating the valuable ZnSe single crystal pieces of a KBr single crystal protect the ZnSe from the sample evaporation. The special holder has an inner vacuum of  $10^{-11}$  torr and an outer space pumped by a turbo pump to reduce the unavoidable small leak at the ZnSe window. A 16 W CO<sub>2</sub> laser is used for heating and melting the small sanidine (feldspar) crystals. The CO<sub>2</sub> laser radiation is focused on a spot of 10  $\mu\text{m}$  diameter, but the area of the laser spot can also be set to heat a larger area ( $\sim 1 \text{ mm}^2$ ) and generally it is preferable to make such an overall heating of each crystal. The special holder for the sample mount can be moved with 1  $\mu\text{m}$  accuracy by a stepmotor in the plane perpendicular to the laser radiation. Thus one can set the irradiation on any of the holes in the sample holder and the measurement of the 20 reference samples and the 24 crystals from Mata Menge can be automatically done over night. A few manual results are taken first in order to check the procedure and to check that the evaporation of argon is adequate for the ion detectors. The heating procedure will be dicussed in chapter 10.

### 9.3 The ultra high vacuum system

The mass spectrometer is a ultra-high vacuum system, pumped with ion getter pumps and prepumped by turbo pumps. Figure 9.3 shows the principle diagram of the mass spectrometer. Valves regulate the various vacuum enclosures electronically and a computer may run a long series of measurements automatically.

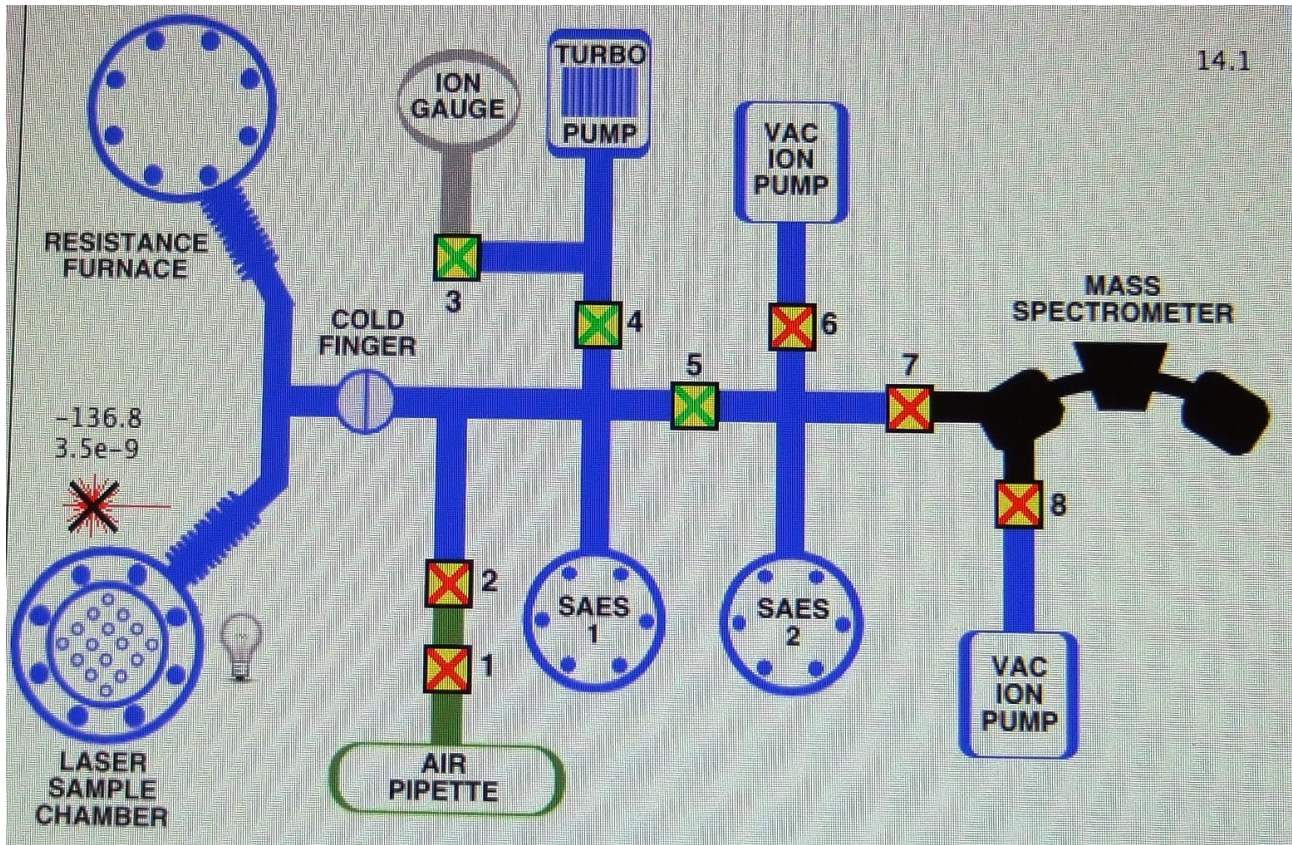


Figure 9.3. Principle diagram of the argon mass spectrometer. Measuring mode.

After loading the feldspar crystals into the laser sample chamber, figure 9.3, the complete vacuum system is pumped with the vacuum sublimation pumps (SAES) and left pumping for more than 1 month to remove as much of the restgas as possible. All tubings are wrapped by heaters to obtain a tubing and copper O-ring temperature of a couple of hundred degrees Celcius during this one month pumping period. Figure 9.4 shows part of the tubing system during this preparation period. The laser sample chamber is heated by a red lamp (se figure 9.4 down to the left) and only taken to about  $100^{\circ}\text{C}$ . The pressure measured by the ion gauges quickly reaches their lower limit of sensitivity ( $\sim 10^{-11}$  torr). The background (blank) pressure is therefore only known to be below this limit.

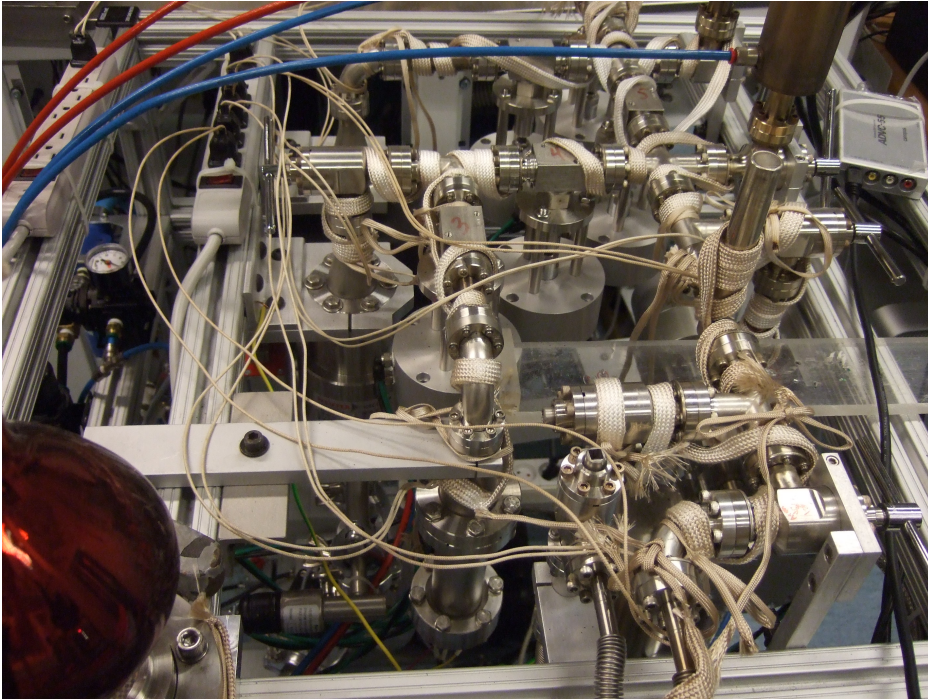


Figure 9.4. A view down into the mass spectrometer gas handling system while heating the stainless steel tubing before measurements start. (Photo: P.E. Lindelof)

#### 9.4 Mass separation and detection

The three key elements of the mass spectrometer at Roskilde University are seen in the photo figure 9.5. The ionization unit and high-voltage accelerator is seen in the front of the photo, the electromagnet which bend the ions is seen to the left and the 4 single ion detectors to the right in the background. The acceleration voltage is a few kV and single electron charged ions are created at a hot cathode. The magnet bends the beam of accelerated ions according to their  $e/m$  ratio, where  $e$  is the electronic charge and  $m$  is the mass of the ions. The ions are bend into one of 3 single ion scintillation counters or a Faraday cup, depending on the fluence of ions. For high fluence the Faraday cup is too sensitive and overloads. Only the scintillation counters are therefore used and to reduce the amount of gas to be measured, only the gas between valve 5, 6 and 7 on figure 9.3 is ionised and measured. Adjusting the current through the electromagnetic allows bending a particular ion mass into a given detector. The different argon isotopes are separated into the three detectors by a calibration using a small amount of atmospheric air, which naturally contains argon isotopes. The atmospheric air is let into the vacuum system through a small pipette shown in figure 9.3. The various argon isotopes ( $^{36}\text{Ar}$ ,  $^{37}\text{Ar}$ ,  $^{38}\text{Ar}$ ,  $^{39}\text{Ar}$ ,  $^{40}\text{Ar}$ ) can be readily separated and each gives a square line shape. However small amount of hydrocarbon ( $\text{HC}_3$ ,  $\text{H}_2\text{C}_3$ ,  $\text{H}_3\text{C}_3$ ,  $\text{H}_4\text{C}_3$ ) will give a small extra contribution, and the calibration of the detection must therefore be changed slightly ( $\sim 0.14$  mass unit) away from the asymmetrical maximum signal on the detector. The ion detector sensitivity is adjusted so that for the detector called “high” a fixed amount of air ( $\sim 1.2 \cdot 10^{-13}$  moles of argon) gives 1 mV corresponding to 60.000 counts/s.  $50 \mu\text{V}$  corresponds to 1200 counts/s in detector “axial” and  $150 \mu\text{V}$  corresponds to 3600 counts/s into detector “low”. As mentioned above the ratio of  $^{40}\text{Ar}/^{36}\text{Ar}$  ( $\sim 302.75 \pm 0.70$ ) from the atmospheric air pipette measurements is considered an almost basic ratio. The ratio must however be corrected due to the so-called fractionation factor induced during the neutron activation. This is a small correction, though. All through our subsequent measurements on the Mata Menge samples, air pipette calibrations are performed regularly.

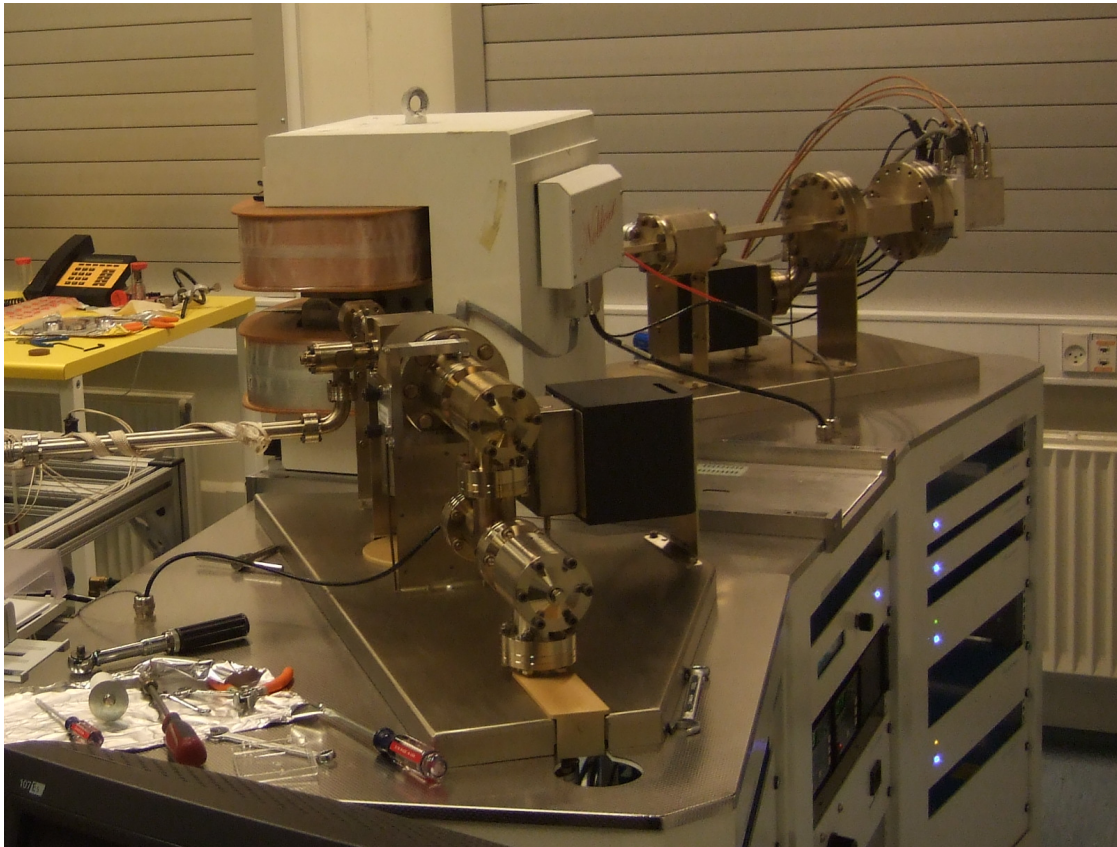


Figure 9.5. Argon mass spectrometer at Roskilde University, From front to back are seen: Gas ionization and acceleration unit,  $e/m$  ion trajectory bending electromagnet, 4 Detectors. (Photo: P.E. Lindelof).

An important check measurement is the so-called “blank”, which is repeated for every measurement and determines the background gas caught in the UHV tubing system. This background argon fluence must be subtracted any of our measurement. This is done by pumping 3 minutes on all tubes, then close off the volume between valve 5, 6 and 7 and finally wait 3 minutes to equilibrium is reached. Valve 7 is then opened for ionization and scintillation detection for three minutes. The result of this background measurement is named a “blank” in the measurement procedure on page 54.

### 9.5 Computer control

All valves, gauges, ionizations, scintillation counters and other electronic equipment are computer controlled and can be followed on the local computer (and a remote computer). Figure 9.6 shows some of the graphs and informations, which can all be simultaneously followed on the computer screen. The diagram over the spectrometer vacuum system shows which valves are closed or open. Earlier data can be displayed together with the present uptake of data and pressure. Since there are only three active scintillation counters, the counting of different argon isotope ions is done in turn. The heatings of the feldspar samples are registered and the formula for calculating the concentration of the various argon isotopes and the calculated age of the sample is displayed with the necessary correction for atmospheric argon and with the background argon subtracted.

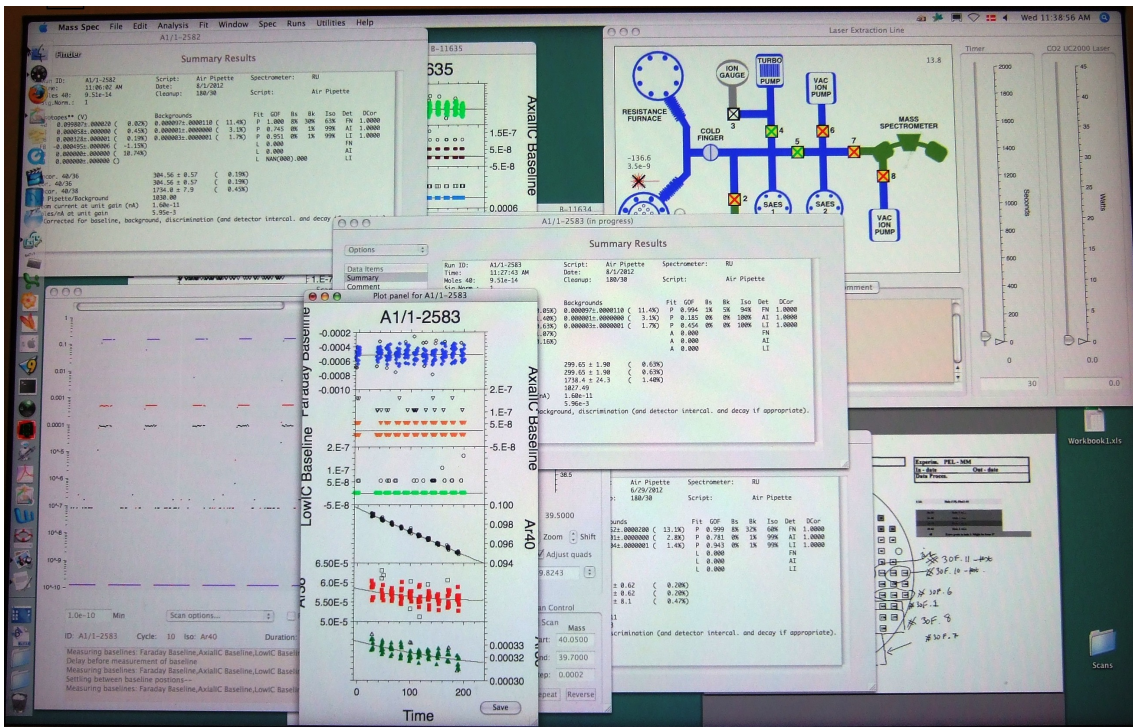


Figure 9.6. Computer screen showing the various software and displays of argon mass spectrometer.

A video screen follows the samples as they are heated individually by the CO<sub>2</sub> laser. This screen is situated in the electronic rack and part of the sample holder (figure 9.1) is seen on figure 9.7. A step motor moves the sample holder in the xy plane and allows a precise position of the position of the CO<sub>2</sub> laser spot on any crystal. The temperature of the sanidine feldspar crystals can be followed on the top electronic rack (1264°C), figure 9.7. The CO<sub>2</sub> laser spot position can be changed by the stepmotor. The size of the laser spot can be regulated and the state of each sanidine crystal can be seen and measured.

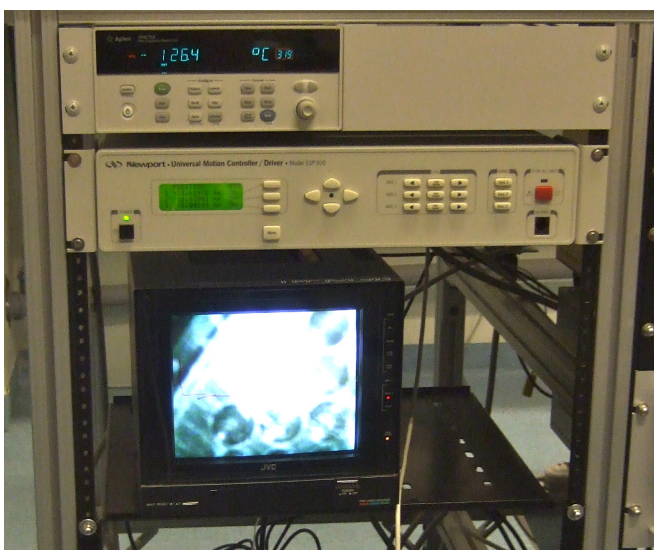


Figure 9.7. Pyrometer temperature display (top electronics, here showing 1264°C) of each individual sanidine crystal in the mass spectrometer crystal mount. Below the electronics for the Servo stepmotor Electronics. Lowest in this photo is the video monitor showing the sanidine crystals in the spectrometer sample holder. (Photo: P.E. Lindelof).

## 9.6 The measurement procedure

The  $^{40}\text{Ar}/^{39}\text{Ar}$  age determination has in principle a very high accuracy compared to other methods relevant to the whole Palaeolithic period (2.5 million years before present (BP) to 12.000 BP). Often the accuracy is better than 1%, but this requires that a number of rules about the material uptake from the ground and the technical mass spectroscopic procedures be fulfilled. In this section I shall only describe the technical procedures in the laboratory. Later (chapter 8) I will describe uncertainties of geological and archaeological nature.

The samples used are feldspar sanidine crystals of  $\frac{1}{2}$  mm average sizes, which contain about 1 atomic % potassium. Such crystals generate amply sufficient radiogenic  $^{40}\text{Ar}$  for determination of an age of 1 million years BP. However there are a number of possible errors, precautions and corrections, which are crucial:

- 1) Did the crystals solidify once or did the solidification occur in several steps in several volcanic eruptions? Different parts of the crystals may therefore display different ages. This may show up as irregularities in the step-heating graphs or the isochron plots. The age may also simply represent an earlier volcanic eruption not corresponding to the stratigraphic layer under investigation.
- 2) The reference sanidine (Alder Creek) determines the J factor. This measurement is done 20 times during the measurements. There are 4 positions for the ACS references in the nuclear reactor, each with 5 reference (ACS) samples. The J value is extrapolated and averaged to the position of the Mata Menge sanidine crystals (2408).
- 3)  $^{38}\text{Ar}$  may transfer into  $^{40}\text{Ar}$  during the neutron irradiation, but this is mostly insignificant
- 4) There is always a small background of argon in the vacuum system. This is most likely to be of the composition corresponding to air. The background is regularly measured (a blank) and this amount of argon gas must be subtracted. The Blancs are measured many times since it may change.
- 5) A pipette amount of argon with air composition is injected into the vacuum system to calibrate regularly the spectrometers sensitivity and isotope calibrations [Lee 1981].
- 6) During each measurement series, the background noise is measured. This also gives a small correction and determines the standard error, which is given by the  $2\sigma$  standard deviation corresponding a confidence probability of 95%. The measurements of the 24 Mata Menge crystals are programmed into the computer and ran over night. Actually only 17 crystals were found suitable or survived the measurement procedure. These 17 results are presented in the next chapter.

# 10. Results on the Sanidine Crystals from Mata Menge

## 10.1 Overview of the 24 sanidine crystals in PL FLO11-01 from Mata Menge

Out of the 3 kg of volcanic tuff/sand material, PL FLO11-01, I have manually picked 24 feldspar ½ mm size crystals containing potassium. These crystals are of the sanidine type and weighed all together only about 50 mg. To obtain a reliable <sup>40</sup>Ar/<sup>39</sup>Ar age determination only one crystal is in principle needed. But this requires of course that this crystal is representative for a stratigraphic layer close to where the archaeological artefacts have been dropped in the first place. Out of the 24 crystals listed in detail in table 10.1, 17 have very satisfactory uncertainties and selfconsistencies. The age results of these 17 crystals are plotted in figure 10.1. They give a weighted average age of 1.05±0.01 million years, if the average is simply taken among these 17 completed age results.

Lab ID#	Relative Isotopic Abundances					Derived Results					Inverse Isochron Data											
	<sup>40</sup> Ar	<sup>39</sup> Ar	<sup>38</sup> Ar	<sup>37</sup> Ar	<sup>36</sup> Ar	<sup>40</sup> Ar/Mo	Ca/K	% <sup>40</sup> Ar	Age (Ma)	w±J	<sup>36</sup> Ar/ <sup>40</sup> Ar	<sup>39</sup> Ar/ <sup>40</sup> Ar	<sup>36</sup> Ar/ <sup>39</sup> Ar									
	±1σ	±1σ	±1σ	±1σ	±1σ	±1σ	±1σ	±1σ	±1σ	±1σ	±%1σ	±%1σ	Er. Corr.									
<b>PL-FLO11-01</b>																						
2408-01	0.091	9E-05	0.005	3E-05	1E-04	4E-06	0.014	2E-04	3E-04	9E-06	0.00	5.69578	0.0935	9.7	1.75573	0.53423	0.53	0.00302	3.28	0.05413	0.53	0.0063
2408-02A	0.215	2E-04	0.088	1E-04	0.001	1E-05	0.001	2E-04	4E-04	9E-06	0.00	0.02303	0.0038	43.3	1.03482	0.03075	0.03	0.00190	2.27	0.40930	0.13	0.0164
2408-02B	0.427	2E-04	0.342	2E-04	0.004	1E-04	0.001	3E-04	3E-04	8E-06	0.30	0.00797	0.0018	80.9	0.98725	0.00718	0.01	0.00064	3.03	0.80126	0.08	0.0095
2408-02C	0.089	9E-05	0.079	9E-05	9E-04	9E-06	4E-04	2E-04	2E-05	8E-06	0.07	0.00903	0.0039	92.2	1.01883	0.02797	0.03	0.00026	32.24	0.88481	0.15	0.0020
2408-02D	0.227	2E-04	0.199	2E-04	0.002	1E-05	9E-04	2E-04	7E-05	8E-06	0.17	0.00854	0.0016	90.2	1.00635	0.01135	0.01	0.00033	10.28	0.87654	0.10	0.0043
2408-02E (fusion str)	0.099	9E-05	0.007	3E-05	1E-04	4E-06	0	2E-04	3E-04	9E-06	0.01	0	0.0426	6.3	0.84673	0.36597	0.37	0.00314	2.90	0.07256	0.43	0.0067
2408-03fusion	1.171	3E-04	0.168	2E-04	0.003	2E-05	8E-04	2E-04	0.003	2E-05	0.15	0.00948	0.0019	14.8	1.00763	0.03318	0.03	0.00285	0.57	0.14385	0.09	0.0140
2408-03fusion2	0.054	7E-05	0.008	3E-05	1E-04	4E-06	8E-04	2E-04	2E-04	7E-06	0.01	0.20411	0.0394	12.1	0.79192	0.26296	0.26	0.00294	4.57	0.14938	0.42	0.0092
2408-04	0.218	1E-04	0.022	3E-05	4E-04	7E-06	0.005	2E-04	6E-04	1E-05	0.03	0.41894	0.0154	12.9	1.25741	0.12786	0.13	0.00292	1.50	0.10007	0.25	0.0112
2408-04B	0.736	3E-04	0.343	2E-04	0.004	2E-05	0.05	4E-04	0.001	1E-05	0.30	0.28527	0.0022	52.3	1.09651	0.01013	0.01	0.00160	1.00	0.46637	0.07	0.0171
2408-04C	1.349	3E-04	0.188	2E-04	0.003	2E-05	0.029	3E-04	0.004	2E-05	0.16	0.30757	0.0032	21.7	1.523	0.03139	0.03	0.00262	0.57	0.13906	0.08	0.0134
2408-04D	0.547	3E-04	0.064	9E-05	0.001	9E-06	0.011	3E-04	0.002	1E-05	0.08	0.33301	0.0078	17.7	1.48787	0.03884	0.06	0.00276	0.85	0.11650	0.15	0.0168
2408-04E	0.922	3E-04	0.088	1E-04	0.002	1E-05	0.013	2E-04	0.003	2E-05	0.08	0.28782	0.0049	16.4	1.67633	0.05582	0.06	0.00280	0.63	0.09586	0.14	0.0116
2408-05	0.122	1E-04	0.006	3E-05	1E-04	4E-06	0.004	2E-04	4E-04	9E-06	0.00	1.26318	0.0697	5.7	1.22643	0.48202	0.48	0.00316	2.36	0.04519	0.46	0.0063
2408-05fusion	0.438	2E-04	0.195	2E-04	0.003	1E-05	0.039	3E-04	7E-04	1E-05	0.17	0.39893	0.0032	50.1	1.09915	0.01681	0.02	0.00167	1.53	0.44561	0.10	0.0134
2408-06	0.047	7E-05	0.004	3E-05	8E-05	4E-06	0.006	2E-04	1E-04	8E-06	0.00	2.56037	0.0953	21.4	2.29892	0.56472	0.56	0.00263	6.69	0.09104	0.61	0.0038
2408-06fusion	0.35	2E-04	0.059	9E-05	9E-04	9E-06	0.09	3E-04	9E-04	9E-06	0.05	2.9635	0.0186	25.4	1.47056	0.0468	0.05	0.00250	1.08	0.16912	0.16	0.0139
2408-07	0.988	3E-04	0.05	8E-05	0.001	1E-05	0.002	2E-04	0.003	2E-05	0.04	0.07599	0.0073	9.6	1.84036	0.12221	0.12	0.00303	0.70	0.05086	0.17	0.0088
2408-07fusion	0.319	1E-04	0.023	6E-05	4E-04	6E-06	0.002	2E-04	9E-04	1E-05	0.02	1.17454	0.0173	19.0	2.53628	0.1355	0.14	0.00271	1.25	0.07330	0.24	0.0064
2408-08	0.03	6E-05	0.005	3E-05	8E-05	5E-06	0.004	2E-04	7E-05	8E-06	0.00	1.58714	0.0625	34.0	1.84257	0.44329	0.44	0.00221	12.41	0.18061	0.62	0.0056
2408-8fusion	0.35	2E-04	0.041	7E-05	7E-04	8E-06	0.05	4E-04	0.001	1E-05	0.04	2.41792	0.0179	11.6	0.97563	0.08376	0.08	0.00296	1.13	0.11675	0.17	0.0186
2408-09A	0.5	3E-04	0.011	2E-05	4E-04	7E-06	0.011	2E-04	0.002	2E-05	0.01	2.05675	0.0369	1.8	0.81224	0.46201	0.46	0.00329	1.04	0.02161	0.42	0.0062
2408-09fusion	0.851	3E-04	0.291	2E-04	0.004	2E-05	0.155	8E-04	0.002	2E-05	0.25	1.04632	0.0053	36.2	1.03562	0.01647	0.02	0.00214	0.90	0.34178	0.06	0.0200
2408-10A	0.029	7E-05	0.004	2E-05	5E-05	5E-06	2E-04	2E-04	7E-05	8E-06	0.00	0.11444	0.0989	28.7	2.28979	0.68664	0.69	0.00329	12.05	0.12237	0.73	0.0060
2408-10fusion	1.108	4E-04	0.323	2E-04	0.004	2E-05	0.001	2E-04	2E-04	8E-06	0.28	0.00651	0.0012	95.6	3.20623	0.00749	0.02	0.00015	4.76	0.29136	0.07	0.0030
2408-11A	0.085	1E-04	0.012	5E-05	2E-04	6E-06	1E-04	2E-04	2E-04	1E-05	0.01	0.01955	0.0322	17.3	1.16772	0.25144	0.25	0.00277	4.49	0.14460	0.45	0.0072
2408-11fusion	0.632	3E-04	0.165	2E-04	0.002	1E-05	9E-04	2E-04	0.002	2E-05	0.14	0.10173	0.0021	25.1	0.94491	0.02675	0.03	0.00251	0.95	0.26023	0.10	0.0167
2408-12A	0.011	4E-05	9E-04	1E-05	4E-06	4E-06	0.002	2E-04	4E-05	9E-06	0.00	4.41207	0.4291	0.0	0	2.9879	2.99	0.00363	23.34	0.08293	1.46	0.0050
2408-12fusion	0.151	1E-04	0.013	4E-05	2E-04	5E-06	0.098	6E-04	2E-04	8E-06	0.14	0.00754	0.0021	50.6	1.02635	0.01819	0.02	0.00165	1.81	0.48219	0.09	0.0134
2408-13A	0.047	9E-05	0.009	5E-05	1E-04	6E-06	0	2E-04	1E-04	1E-05	0.01	0	0.0428	12.4	0.61012	0.30732	0.31	0.00293	7.12	0.19867	0.29	0.0050
2408-13fusion	1.396	4E-04	0.267	2E-04	0.004	2E-05	0.008	2E-04	0.004	2E-05	0.23	0.05786	0.0016	19.6	1.00182	0.02199	0.02	0.00269	0.53	0.19156	0.08	0.0201
2408-14A	0.005	4E-05	0.001	2E-05	2E-05	5E-06	0.004	2E-04	0	8E-06	0.00	5.74648	0.3487	116.2	4.25353	1.84535	1.85	0.00000	0.00	0.26703	1.78	0.0011
2408-14fusion	0.064	7E-05	0.004	2E-05	9E-05	4E-06	0.035	3E-04	2E-04	8E-06	0.00	16.2101	0.1661	4.2	0.62885	0.56254	0.56	0.00321	3.92	0.06530	0.50	0.0062
2408-15A	0.012	5E-05	0.006	4E-05	8E-05	5E-06	6E-05	2E-04	0	9E-06	0.01	0.01932	0.0613	109.8	2.03916	0.39525	0.40	0.00000	0.00	0.52649	0.73	0.0012
2408-15fusion	0.342	2E-04	0.165	1E-04	0.002	1E-05	6E-04	2E-04	6E-04	1E-05	0.14	0.00754	0.0021	50.6	1.02635	0.01819	0.02	0.00165	1.81	0.48219	0.09	0.0134
2408-17A	0.008	4E-05	0.006	3E-05	8E-05	5E-06	0.005	2E-04	9E-06	7E-06	0.01	1.72247	0.0604	72.4	0.98847	0.34036	0.34	0.00092	90.41	0.17661	0.68	0.0036
2408-17fusion	0.187	1E-04	0.039	7E-05	6E-04	7E-06	0.031	3E-04	5E-04	9E-06	0.03	1.53594	0.0146	21.2	1.00369	0.06969	0.07	0.00264	1.86	0.26030	0.19	0.0103
2408-18A	0.005	3E-05	0.002	1E-05	3E-05	4E-06	5E-04	2E-04	7E-07	6E-06	0.00	0.59402	0.1869	96.9	2.97976	1.03794	1.04	0.00100	1098.08	0.31799	1.00	0.0003
2408-18fusion	1.616	5E-04	0.186	2E-04	0.003	2E-05	0.053	4E-04	0.005	2E-05	0.16	0.55246	0.0041	13.1	1.14144	0.03469	0.04	0.00291	0.47	0.11532	0.09	0.0194
2408-19A	0.101	1E-04	0.043	7E-05	6E-04	7E-06	1E-04	2E-04	2E-04	8E-06	0.08	0.00673	0.0074	40.3	0.9126	0.0513	0.05	0.00200	3.79	0.43172	0.18	0.0140
2408-19B	0.193	1E-04	0.175	2E-04	0.002	1E-05	2E-04	2E-04	9E-06	7E-06	0.15	0.00212	0.0018	98.6	1.06608	0.01242	0.01	0.00005	81.20	0.90458	0.10	0.0004
2408-19C	0.162	1E-04	0.144	1E-04	0.002	1E-05	1E-04	2E-04	3E-05	8E-06	0.13	0.00198	0.0022	91.3	1.06481	0.01562	0.02	0.00029	16.19	0.88853	0.12	0.0030
2408-19D	0.292	2E-04	0.235	2E-04	0.003	2E-05	4E-05	2E-04	1E-04	8E-06	0.01	0.00036	0.0016	87.8	1.06837	0.00984	0.01	0.00041	6.53	0.80341	0.10	0.0046

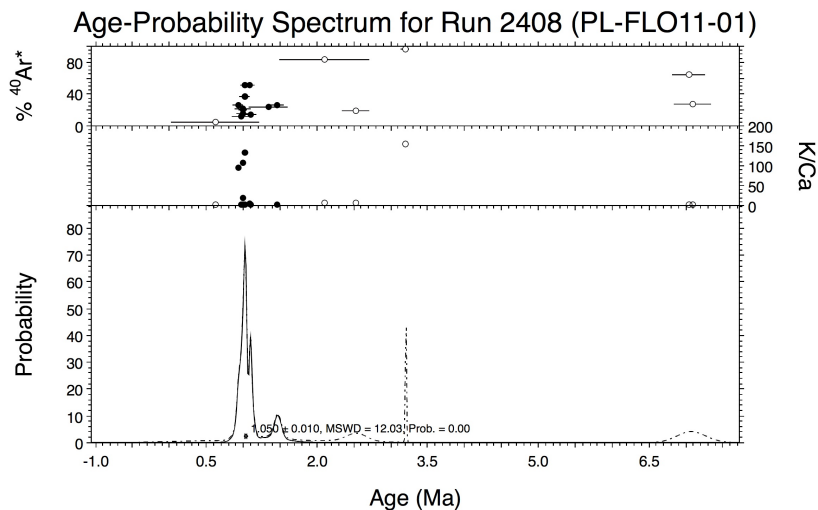


Figure 10.1. The probability of the different ages versus age for all samples. The 17 most reliable crystals, judged from their isochron and uncertainty is plotted and smoothed. The top graph shows the relative amount of radiogenic argon vs. age. The middle graph shows the relative amount of potassium/calcium. The amount of calcium is important because a small amount of argon can be generated by the neutron irradiation.

The 17 sanidine sample crystals, which are selected because of their reliability and consistency, are shown in a fused isochron plot figure 10.2. Only few of the stepheating results lie outside the isochrone line. These deviations are explained by double heating during the volcanic eruption or inhomogeneous diffusion conditions inside some crystals. The isochron plot yields the basic air ratio  $^{36}\text{Ar}/^{40}\text{Ar}$  at the isochrones line's crossing with the ordinate axis. The slope of the isochrone line and the abscissa value of the extrapolated isochrone line both give independently the value of the age, within an estimated uncertainty. The combined average values of these many individual age determinations gives an age of  $0.997 \pm 0.017$  Ma BP (figure 10.2), which is slightly lower than an average of the 17 crystals already averaged individually, namely  $1.050 \pm 0.010$  (figure 10.1). This last average age is the most accurate, because the most reliable crystals will have the highest probability weight. This age determination is the most accurate obtained by the spectrometer ever.

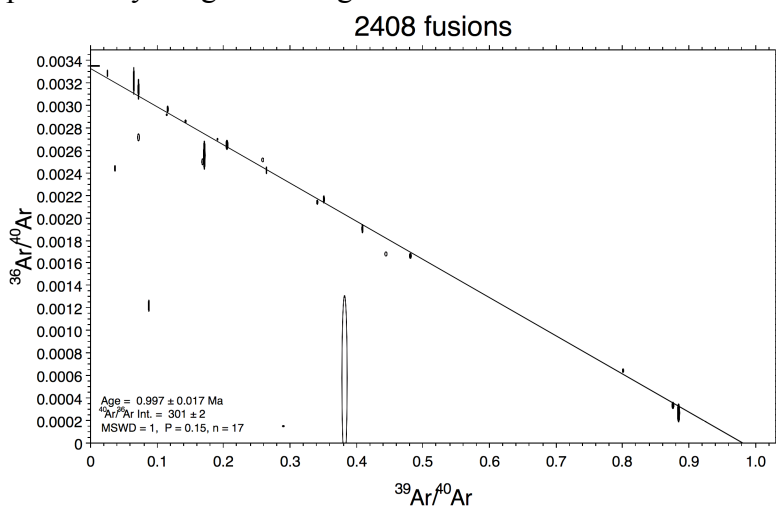


Figure 10.2. Isochrone plot of the 17 most consistent and accurate crystals. In calculating the average age less weight is put on the most inaccurate argon determination and the final average is from weighted slope and abscissa crossing of the line. This gives the age  $0.997 \pm 0.017$  Ma BP.

### 10.2 The 3 most excellent age determinations

There are many ways of taking the average of the ages of individual results produced by a release of argon from a heating. Some of the individual results will often be outside the error range of the rest. However each individual result is indeed correct within its own error limits. The reason that the individual measurement do not overlap is that the argon release vary due to crystal inhomogeneity, a history of the crystal, which is shorter than the diffusion time leading to inhomogeneous argon from the atmosphere or a double heating of the crystals in a long volcanic eruption. Finally of course a background in the spectrometer or a generation of argon in the nuclear reactor may be important, but this is almost always of minor importance.

Run ID	Sample	% radiogenic	Age (Ma)	error
2408-22C	PL-FLO11-01	27,7	1,02467	0,03580
2408-22B	PL-FLO11-01	35,4	0,98599	0,02775
2408-19E	PL-FLO11-01	82,0	1,06882	0,01245
2408-19D	PL-FLO11-01	87,8	1,06837	0,00984
2408-19C	PL-FLO11-01	91,3	1,00481	0,01562
2408-19B	PL-FLO11-01	98,6	1,06608	0,01242
2408-02D	PL-FLO11-01	90,2	1,00635	0,01135
2408-02C	PL-FLO11-01	92,2	1,01883	0,02797
2408-02B	PL-FLO11-01	80,9	0,98725	0,00718

*Table 10.2.  $^{40}\text{Ar}/^{39}\text{Ar}$  results for several heating steps of three sanidine crystals, which have a high degree of consistency as judged from the isochrones plots. In the series of step heatings, the results for the first and the last heating step have been omitted because the first and the last heating steps are always the most uncertain. The average age of the nine step-heating results are shown in the table with their estimated errors. Assuming that all these ages really represent the same age, we may calculate the average age and the combined error:  $1.0272 \pm 0.0042$  Ma BP.*

In table 10.2 we have selected only 9 heating steps of 3 crystals, which all have a excellent internal constancy as judged from their isochron plots. In table 10.2 we have omitted the first and the last heating steps, since these may represent the surface of the crystal or the extraordinarily strongly bound argon. A strict average calculation of these 9 data sets gives an age of  $1.0272 \pm 0.0042$  Ma BP. This I suggest to be the best age value for the material PL FLO11-01 in trench no. 18, the layer just above the sheet flow layer with the artefacts and the fossils.

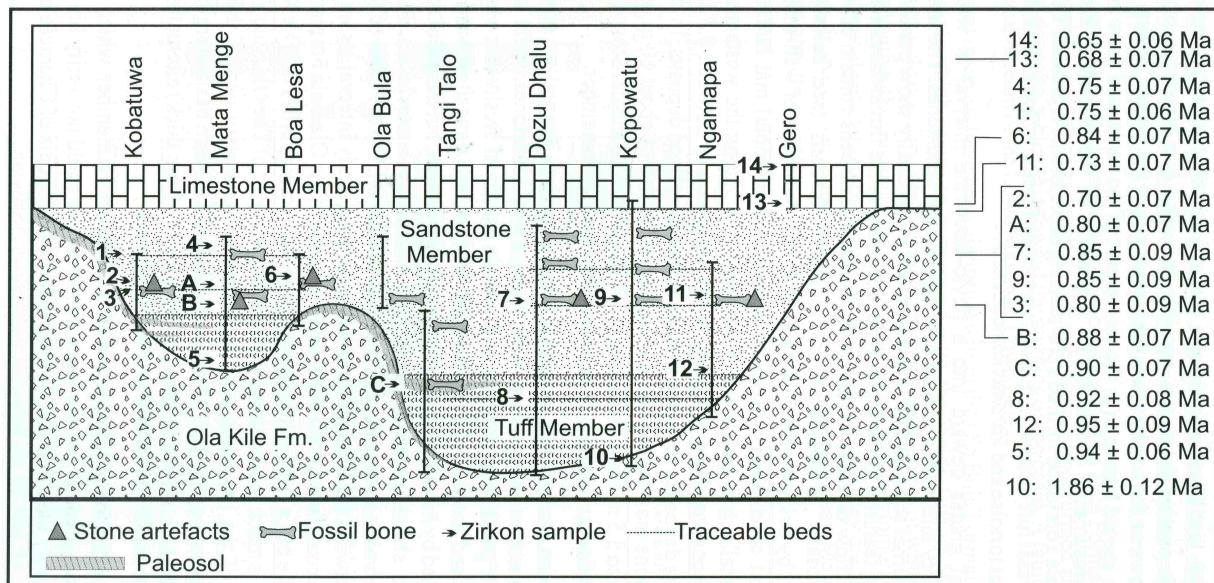
An average of the age determination based on table 10.2 and the figures 10.1 and 10.2 give the age  $1.02 \pm 0.02$  Ma BP.

### 10.3 Earlier dating results in Soa Basin and the present status.

Prior to the  $^{40}\text{Ar}/^{39}\text{Ar}$  dating in this work and the work by Gitte M. Jensen [Brumm et al. 2010a], the chronology of the Soa Basin layers were based on palaeomagnetism, palaeozoology and fission track measurements. The first dating of soa Basin was based on archaeozoological dating of Pygmy stegodon (elephants), Komodo dragons and giant tortoises [Maringer et al. 1970a, 1979b]. The observation of the palaeomagnetic reversal gave a chronological fixpoint of 760.000 years BP. All archaeological layers with artefacts are definitely later than this age, as already emphasized by Verhoeven [1953] and Maringer et al. [1970a, 1970b].

O’Sullivan et al. [2001] and Suminto et al. [2009] have performed fission track measurements at a few of the archaeological sites in the Soa Basin including Mata Menge. Figure 10.3 gives an overview of these fission track determinations at some sites marked on the map figure 5.1. Human artefacts are claimed to be from the period 0.73-0.88 Ma BP with an error margin of 10%. The only site out of the 15 studied in Soa Basin without artefacts (but with fossil animal bones) is Tangi Talo, which was found by fission track to be 0.92 million years old. Our  $^{40}\text{Ar}/^{39}\text{Ar}$  results give an age of 1.02 Ma at the Mata Menge site and Gitte M. Jensen’s  $^{40}\text{Ar}/^{39}\text{Ar}$  results also gave an age of the artefacts at Wolo Sege of 1.02 Ma BP.

Figure 10.3. An attempt by Suminto et al. [2009] on the basis of O’Sullivan et al. [2001] to give an



overview of the chronology of Soa Basin based on fission track data.

The  $^{40}\text{Ar}/^{39}\text{Ar}$  results give a considerably older age for the finds at Wolo Sege and Mata Menge than was earlier believed. If layers are moved around by water or by earthquake, their chronology may be changed; this is called rework. Rework interferes with both the fission track and the  $^{40}\text{Ar}/^{39}\text{Ar}$  dating results. If the tuffaceous layer, where the crystals for both fission track and sanidine for the  $^{40}\text{Ar}/^{39}\text{Ar}$  measurements were found, came with the streaming water from layers higher up in the landscape, then the dating may derive from an earlier tuffaceous layer, and the artefacts are not as old as 1.02 Ma BP. If on the other hand the flow sheet layer of the artefact has come from higher layers in the Soa Basin, then the artefact can be older than our  $^{40}\text{Ar}/^{39}\text{Ar}$  determination shows. There is no doubt that the flow sheet layer with the artefact comes from somewhere else. However as observed by Brumm et al. [2010b], the stone tools have no sign of being water polished, so it is unlikely that they have been taken very far. The likelihood that the tuffaceous layers around the artefact layer is fluvio-deposited is small, since the layer thickness originally had a fairly constant thickness over the 2000 m<sup>2</sup> excavation in Mata Menge and no clear turbulence is observed. Studies of the distribution of stone sizes could help indicate the water flow. In spite of the fact that artefact densities at higher altitudes in the Soa Basin landscape is extremely small it would be worthwhile to look for this to get an unperturbed age determination.

Figure 10.3 is a geological layer chronology made on the basis of fission track data alone. Most of the archaeological sites have been included. The age variations among the archaeological sites are between 0.73 and 0.88 Ma BP. These fission track data are thus within their individual error bars. The new  $^{40}\text{Ar}/^{39}\text{Ar}$  data are 20% older than the fission track data and it seems therefore that a

new overall chronology diagram is required instead of figure 10.3. Before such a new diagram is made, however, some of the other archaeological site in Soa Basin should be measured with the accurate  $^{40}\text{Ar}/^{39}\text{Ar}$  dating method.